A THREE-DIMENSIONAL (3D) STRUCTURAL MODEL FOR AN OIL-PRODUCING BASIN OF THE BRAZILIAN EQUATORIAL MARGIN

Maia de Almeida, Narelle[1*]; Alves, Tiago M.[2]; Nepomuceno Filho, F. [3]; Freire, George Satander Sá[1,4]; Souza, Ana Clara B.[4]; Leopoldino Oliveira, Karen M.[4]; Normando, Márcio Nunes[4]; Barbosa, Thiago Henrique S.[5]

[1] Departamento de Geologia, Universidade Federal do Ceará (UFC), Campus do Pici, Bloco 912, Fortaleza, Ceará, CEP 60440-554, Brasil. Emails: narelle@ufc.br (*corresponding author), freire@ufc.br

[2]Cardiff University. 3D Seismic Lab, School of Earth and Ocean Sciences, Cardiff University, Cardiff, United Kingdom. Email: alvest@cardiff.ac.uk

[3] Departamento de Física, Universidade Federal do Ceará (UFC), Campus do Pici, Bloco 922, Fortaleza, Ceará, CEP 60440-554, Brasil. Email: nepomuceno@fisica.ufc.br

[4] Programa de Pós-Graduação em Geologia, Universidade Federal do Ceará (UFC), Campus do Pici, Bloco 912, Fortaleza, Ceará, CEP 60440-554, Brazil. Emails: anaclarageologia@alu.ufc.br, karenleopoldino@gmail.com, mnormando@gmail.com

[5] Departamento de Engenharia do Petróleo, Universidade Federal do Ceará (UFC), Campus do Pici, Bloco 709, Fortaleza, Ceará, CEP 60440-554, Brasil. Email: thiagohenrique@alu.ufc.br

ABSTRACT

Hydrocarbon discoveries in regions such as the Brazilian Equatorial Margin, Equatorial Africa and French Guiana have recently confirmed their importance as new exploration frontiers. The Mundaú sub-basin, located on the Brazilian Equatorial Margin, is an oil and gas producing region with four producing fields in shallow water: Xaréu, Atum, Espada e Curimã. In order to understand the structural and seismic-stratigraphic frameworks of an oil-producing area of the Brazilian Equatorial Margin, this work addresses the 3D geometry and

spatial distribution of main faults in the Curimã and Espada fields. The occurrence of hydrocarbons in the Mundaú sub-basin is compared with fields in other parts of the Brazilian Equatorial Basin, and in Equatorial Africa. Data from 12 wells and a 3D post-stack time-migrated multichannel seismic volume are used to define nine (9) main seismic-stratigraphic units: the syn-rift Mundaú Formation (Units 1, 2, 3 and 4); the transitional Paracuru Formation (Unit 5) and the drift Ubarana (Uruburetama and Itapagé Members, Units 6 and 7), Tibau and Guamaré Formations (Units 8 and 9). The study area is dominated by NW-SE planar normal faults, basinward-dipping, that formed multiple half-grabens and tilted blocks with small anticlines and synclines genetically related to a transtensional system. Three types of plays are recognised in the Mundaú sub-basins: structural, combined (structural-stratigraphic) and stratigraphic (turbiditic). In the eastern part of the region where the basement is shallow, no oil was found. Conversely, oil was discovered in an anticlinal trap formed on a hanging-wall block analogous to fields in Côte D'Ivoire-Ghana transform margin. This work shows that combined traps on footwall blocks are successful plays near the shelf break of the Mundaú sub-basin, in similarity with the Espoir and Baobab fields in Ivory Coast Basin. Furthermore, turbiditic reservoirs in drift units are analogous to the Stabroek block in Guyana and prospects in the Gulf of Guinea. The structural and petroleum-play analyses in this work are therefore crucial to understand the multiple geological processes leading to the trapping of hydrocarbons in the larger Equatorial Atlantic Ocean.

Keywords: Atlantic Ocean; Equatorial Brazil; Ceará Basin; 3D seismic; oil fields; 3D modelling.

1. INTRODUCTION

The Ceará Basin is located on the Brazilian Equatorial Margin (BEM) between the Potiguar Basin to the southeast and the Barreirinhas Basin to the northwest (Fig. 1). The BEM developed as a typical continental margin of the transform type (Matos, 2000). The bulk of its development was dominated either by oblique extension (transtension) or by pure and simple shear movements, all responding to a dominant dextral sense of movement in transfer (syn-rift) and transform (post-rift) faults. In this portion of the late Gondwana supercontinent, continental rupture and breakup took place in an East-West direction, creating shorelines with two predominant directions: NW-SE in transtensional portions, and E-W in purely transcurrent portions (Zalán, 2015).

The Ceará Basin has been considered, since the 1970's, a modest oil and gas producer in shallow water, where production rates have reached only a few thousands of boe/d. In contrast, the neighbouring Potiguar Basin recorded significant yields during the 1990s, with its onshore fields reaching a production rate of ~100,000 boe/d. The onshore portion of Barreirinhas Basin also reached production rates of a few tens of thousands of boe/d into the 1980s. However, there is no significant production in this basin at present, as well as in other basins of the BEM such as Pará-Maranhão and Foz do Amazonas (ANP, 2020) (Fig. 1). More recently, in 2012, Petrobras (Petróleo Brasileiro SA) drilled the Pecém well to announce the first ever deep-water oil discovery in the Ceará Basin. Subsequently, Maia de Almeida et al. (2020) proved that reservoirs in the Pecém well comprise Cretaceous sandstones in a combined trap related to both an erosional unconformity and a normal fault. Leopoldino Oliveira et al. (2020) later identified a series of potential stratigraphic and structural traps, and associated petroleum plays, in rift and drift sequences of the Ceará Basin.

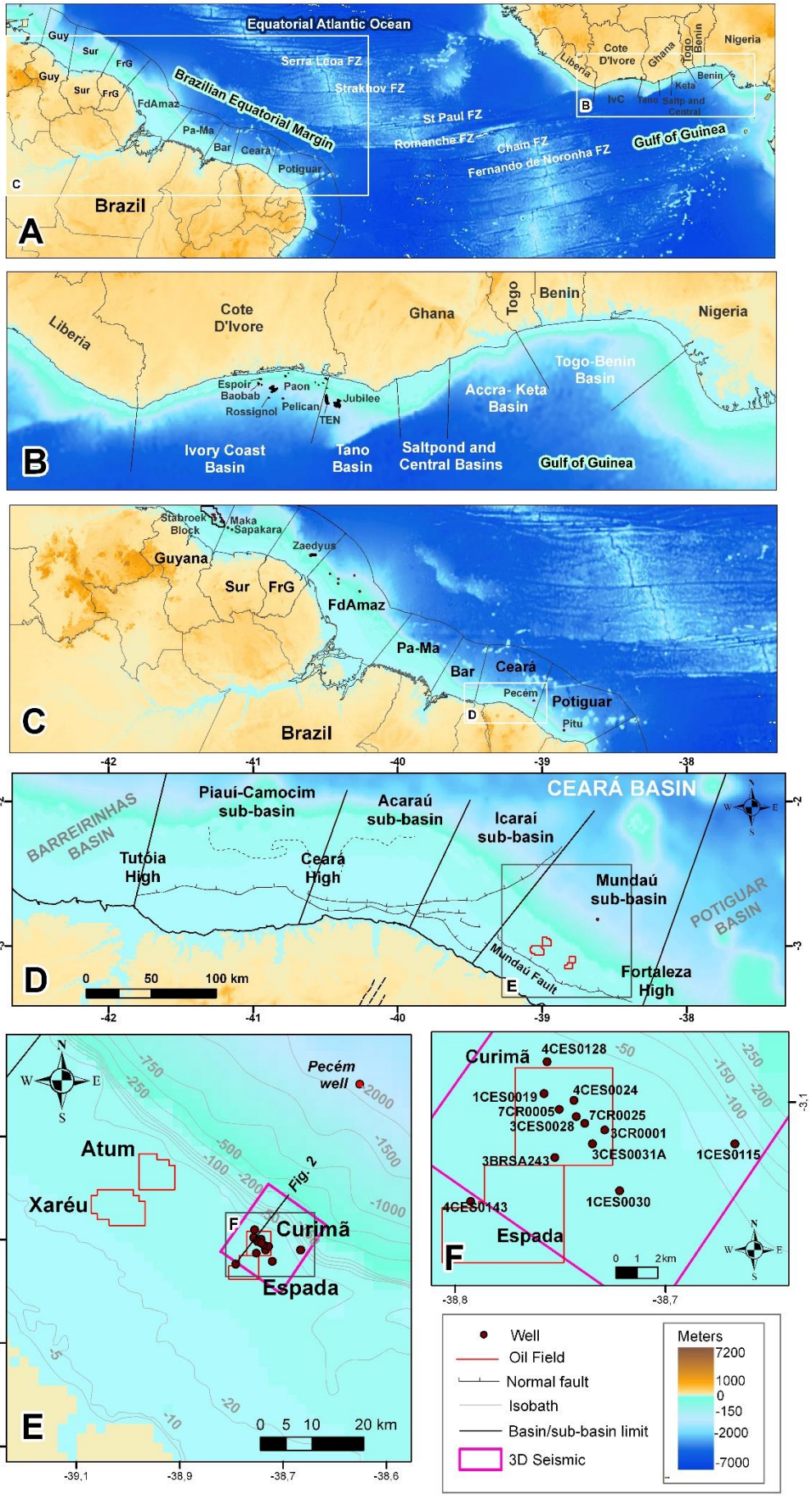
Equatorial Atlantic Ocean
Guy
Sur
FrG
Guy
Sur
FrG
FdAmaz
Pa-Ma
Bar
Ceará
Potiguar
Brazilian Equatorial Margin
Serra Leoa FZ
Strakhov FZ
St Paul FZ
Romanche FZ
Chain FZ
Fernando de Noronha FZ
Gulf of Guinea
C
Brazil
A
Cote D'Ivore
Ghana
Togo
Benin
Nigeria
Liberia
IvC
Tano
Keta
Saltp and Central
B
Liberia
Cote D'Ivore
Ghana
Togo
Benin
Nigeria
Espoir
Baobab
Rossignol
Paon
Pelican
Jubilee
TEN
Togo-Benin Basin
Accra- Keta Basin
Ivory Coast Basin
Tano Basin
Saltpond and Central Basins
Gulf of Guinea
B
Stabroek Block
Maka
Sapakara
Zaedyus
Guyana
Sur
FrG
FdAmaz
Pa-Ma
Bar
Ceará
Pecém
Potiguar
Pitu
D
C
Brazil
-42
-41
-40
-39
-38
-2
-3
BARREIRINHAS BASIN
Piauí-Camocim sub-basin
Acaraú sub-basin
Icaraí sub-basin
CEARÁ BASIN
Tutóia High
Ceará High
Mundaú sub-basin
POTIGUAR BASIN
Mundaú Fault
Fortaleza High
E
D
0 50 100 km
-42
-41
-40
-39
-38
-2
-3
N
W
E
S
Pecém well
-750
-250
-2000
-1500
-1000
-500
-100
-200
Atum
Xaréu
Fig. 2
F
Curimã
Espada
-5
-10
-20
0 5 10 20 km
E
-39,1
-38,9
-38,7
-38,6
-2,9
-3,1
-3,3
-3,4
Curimã
4CES0128
-50
-250
-150
-200
-100
1CES0019
4CES0024
7CR0005
7CR0025
3CES0028
3CR0001
3CES0031A
3BRSA243
1CES0115
1CES0030
4CES0143
Espada
F
0 1 2km
-38,8
-38,7
-3,1
Well
Oil Field
Normal fault
Isobath
Basin/sub-basin limit
3D Seismic
Meters
7200
1000
0
-150
-2000
-7000

Figure 1. A) Map of the Equatorial Atlantic Ocean highlighting the fracture zones and the marginal basins (Guy: Guyana, Sur: Suriname, FrG: French Guiana, FdAmaz: Foz do Amazonas, Pa-Ma: Pará-Maranhão, Bar: Barreirinhas, IvC: Ivory Coast, Saltp: Saltpond). B) Gulf of Guinea basins and their oil fields and discoveries correlated with this work. C) Fields and discoveries of the Brazilian Equatorial Margin, French Guiana, Suriname and Guyana. D) The Ceará Basin sub-divided into four sub-basins: Piauí-Camocim, Acaraú, Icaraí and Mundaú. The study area is located in the Mundaú sub-basin. Structural data was compiled from Zalán and Warme (1985) and Morais Neto et al. (2003). The basins boundaries were provided by the Brazilian National Agency of oil, gas and biofuels (ANP) and boundaries of sub-basins were based on Morais Neto *et al.* (2003). E) Relative location of the four producer fields (Xaréu, Atum, Curimã and Espada) of the Mundaú sub-basin. The location of the wells and 3D seismic data are shown. F) Details of the well data used in this study, as provided by the ANP. The topographic model in the figure was provided by NOAA (ETOPO1).

The first deep-water discovery in Potiguar Basin occurred in 2013 with the drilling of the Pitu well. Soon after, the Brazilian Agency of Petroleum (ANP) opened new exploratory opportunities in structured sandstones of Aptian age, and in Upper Cretaceous, Paleogene and Neogene turbidite sequences, within the Potiguar Basin (ANP, 2018).

On the African conjugate margin of the BEM, the Gulf of Guinea Province (Côte d'Ivoire, Ghana, Togo, and Benin), including the western part of the coast of Nigeria, relatively little hydrocarbon exploration occurred until the 1990s. Until 1995, most discoveries were located in water depths of less than 500 m (Brownfield and Charpentier, 2006). In the 2000s, new discoveries in deep-water areas of Equatorial Africa were made public. The first deep-water in Equatorial Africa was the Baobab field in Ivory Coast (2005). Two years later, the discovery of the giant Jubilee field, offshore Ghana, drew attention to the whole of the Equatorial Atlantic as a major hydrocarbon province. The Jubilee field is now producing more than 100,000 boe/d and has a planned peak production of 120,000 boe/d (Dailly et al., 2017). Further increasing the importance of the Equatorial Atlantic as a petroleum province, the Tweneboa-Enyenra-Ntomme (TEN) fields in Ghana's deep-water were discovered between 2009 and 2012, and began producing oil in 2016 at relatively large rates of 80,000 boe/d.

Offshore French Guyana, significant discoveries have included the Zaedyus Field (2011) with recoverable reserves of 130×10^6 toe (Huaicun, 2014), and the Lisa field of the Stabroek Block, drilled in 2015, this latter comprising potential recoverable reserves of 109 to 191×10^6 toe (OGJ, 2016). Other successful discoveries in the Stabroek Block included the

111 Payara, Liza deep, Snoek and Turbot fields (2017), the Ranger, Pacora, Longtail, Hammerhead
112 and Pluma fields (2018), the Tilapia, Haimara, Yellowtail and Tripletail fields (2019); and the
113 Mako field of 2020 (Exxon Mobil, 2020). More recently, the Maka and Sapakara discoveries
114 offshore Suriname led to the identification of at least seven distinct play types (Offshore, 2020).
115 Most oil and gas discoveries on Equatorial margins of the Central Atlantic are
116 associated with the presence of stratigraphic traps in turbidites. Structural and combined traps
117 are also present (Dailly et al., 2017; Jianping et al., 2010; Kelly and Doust, 2016; Maia de
118 Almeida et al., 2020; Tetteh, 2016; Yang and Escalona, 2011). In such a setting, faults have an
119 important role with regards to controlling oil migration from source intervals to main
120 reservoirs. Faults can act as either conduits or barriers for hydrocarbon migration because they
121 have anisotropic flow properties owing to their complicated three-dimensional structure (Jiang
122 et al., 2015). Thus, a predictive knowledge of fault zone structure and transmissibility can have
123 an enormous impact on the economic viability of new exploration targets, resulting in
124 significant benefits during reservoir management. Understanding the effects of faults and
125 fractures on fluid flow behaviour and distribution within hydrocarbon provinces has, therefore,
126 become a priority in many an offshore prospect (Knipe et al., 1998).
127 Costa et al. *(*1990) have shown that hydrocarbon plays in the shallow water of the Ceará
128 Basin are of the stratigraphic (turbiditic), combined (structural-stratigraphic) and structural
129 types. Structural plays may be classified as rotational, transpressional, transtensional or
130 footwall-related. In addition, Pessoa Neto (2004) showed that the Atum and Curimã oil fields
131 in the Mundaú sub-basin comprise classical examples of combined traps generated by the
132 erosional truncation of tilt blocks limited by normal faults. Though Pessoa Neto (2004) was
133 able to demonstrate that hydrocarbon traps are usually of the mixed type (structural-
134 stratigraphic), and others several structural interpretations have been proposed for the area
135 based on 2D seismic data (Costa et al., 1990; Matos et al., 1996; Morais Neto et al., 2003;

136 Antunes, 2004; Pessoa Neto, 2004; Medeiros et al., 2007; Antunes et al., 2008; Maia de
137 Almeida et al., 2020; Leopoldino Oliveira et al., 2020), the geometry and distribution of
138 subsurface faults is still poorly known in the larger Ceará Basin. Against such a backdrop, this
139 work aims at recognising the 3D geometry and spatial distribution of faults in the Mundaú sub-
140 basin, Ceará Basin, and explain their control on the occurrence of hydrocarbons in the area
141 encompassing the Curimã and Espada fields (Fig. 1). The results will be compared to other
142 basins of the BEM and Equatorial Africa. Three-dimensional (3D) seismic data and a suite of
143 exploration wells are used to address four fundamental research questions:

144 a) What are the typical fault geometries in the Curimã and Espada fields? How are they
145 distributed in these two subsurface prospects?
146 b) How structural elements in the Mundaú sub-basin fit within the regional context of
147 continental rifting of the Equatorial Atlantic Ocean?
148 c) In what way(s) these structures influence local petroleum plays and subsequent
149 hydrocarbon accumulations in an economically significant region of Equatorial
150 Brazil?
151 d) How the present findings compare with similar petroleum basins elsewhere in
152 Equatorial areas of the Central Atlantic?

153

154 Significant advances in mapping structural and stratigraphic features in the Mundaú
155 sub-basin are presented in this work. The possibility of replicating the successful plays mapped
156 in this work in other parts of the BEM, as well as in Equatorial Africa, is demonstrated in the
157 following sections.

158

159 **2. GEOLOGICAL SETTING**

160

The Brazilian Equatorial Margin is related to the opening of the Central Atlantic Ocean, itself formed by the fragmentation and continental breakup of northwest Gondwana during the Lower Cretaceous. During this time, a transtensional shear corridor with a dextral sense of movement was developed at the loci of the present-day north and northern continental margins of Brazil (Azevedo, 1991).

The BEM is characterized by the presence of east-west and northwest-southeast margin segments, forming *en echelon* structures that are typically associated with the predominant strike-slip tectonics of transform margins (Gorini, 1993). It includes, from east to west, the Potiguar, Ceará, Barreirinhas, Pará-Maranhão and Foz do Amazonas basins. The main characteristics of the BEM's offshore basins are: a) their relatively late continental breakup when compared to the Eastern Brazilian Margin (EBM) (Françolin and Szatmari 1987, Szatmari et al., 1987; Matos, 2000), b) a continental breakup stage controlled by strike-slip tectonics with predominant dextral kinematics (Matos, 2000; Basile et al., 2005), c) diachronous subsidence and uplift events on each margin segment controlled by divergent, transtensional or transpressional tectonics (Mohriak, 2003; Zálan, 2004), d) sub-basins that record contrasting histories in terms of their thermal, depositional, magmatic and deformation histories (Milani et al., 2000), and e) the absence of a transitional evaporitic sequence of Aptian age, as well as the absence of structures and sedimentation associated with salt tectonics (Mohriak, 2003; Zálan, 2004; Pellegrini and Severiano Ribeiro, 2018).

The Ceará Basin presents transpressional and transtensional segments and, because of its distinct tectonic character along and across the BEM, it has been previously divided into four distinct sub-basins (Morais Neto et al., 2003).

2.1. Ceará Basin

The Ceará Basin is bounded to the east by the Fortaleza High, to the west by the Tutóia High, to the south by crystalline basement, and to the north by the Romanche Fracture Zone (RFZ) (Costa et al., 1990) (Fig. 1). The basin has been divided into four distinct sub-basins, from east to west, reflecting their different structural style: the Mundaú, Icaraí, Acaraú and Piauí-Camocim sub-basins (Morais Neto et al., 2003) (Fig. 1B). The Piauí-Camocim is separated from the Acaraú sub-basin by the Ceará High. The Acaraú and Icaraí sub-basins have, as common limit, the Sobral-Pedro II lineament. In addition, the Icaraí is separated from the Mundaú sub-basin by an important change in fault trends (Morais Neto et al., 2003). According to Matos (2000), deformation in the Mundaú sub-basin was essentially transtensional in nature, while the Piauí-Camocim sub-basin records one of the most important examples of transpressional deformation on the BEM, with compressive structures such as folds and thrust faults well developed there (Zalán and Warme, 1985).

Beltrami et al. (1994) suggested differences in the sedimentary record of the Mundaú, Icaraí-Acaraú and Piauí-Camocim sub-basins. The Piauí-Camocim sub-basin shows the less complete sedimentary fill of the three sub-basins, with unconformities and depositional hiatuses of greater magnitude. The most complete stratigraphic record is that of the Mundaú sub-basin (Fig. 2).

2.2. Mundaú sub-basin

The Mundaú sub-basin is a hydrocarbon-producing region with four oil and gas fields in its shallow waters: Xaréu, Atum, Curimã and Espada (Fig. 1). According to ANP (2020), this basin produced 4,109 bbl/d oil and 83 Mm³/d gas, totalling 4,632 boe/d. Matos et al. (1996) have demonstrated that faults delimiting the Mundaú sub-basin reveal significant changes in geometry, varying from ‘planar’ to ‘listric’, ‘sigmoidal-listric’ and ‘listric with a

211 flat-ramp profile'. In addition, they proposed three distinct architectures for the Mundaú sub-
212 basin: 1) tilt blocks where the Mundaú Fault shows a planar or listric geometry at depth, 2) tilt
213 blocks with a synclinal next to the Mundaú Fault due to its sigmoidal geometry, and 3) tilt
214 blocks with anticlines and small synclines genetically related to the flat-ramp geometry of the
215 Mundaú Fault. According to Antunes et al. (2008), the structural framework of the Mundaú
216 sub-basin is dominated by a normal fault, the Mundaú Fault, which strikes NW-SE and dips to
217 the NE (Fig. 1).

218 The tectono-sedimentary evolution of the Mundaú sub-basin consists of three
219 major megasequences (Beltrami et al., 1994): syn-rift, transitional and drift. The syn-rift phase
220 is characterized by the development of NW-SE normal faults bounding asymmetric half-
221 grabens, and continental sedimentation marked by fluvial-deltaic sandstones and shales of the
222 Mundaú Formation (Beltrami et al., 1994) (Fig. 2). The top of this unit is a regional
223 stratigraphic horizon, called Electric Mark 100 (Costa et al., 1990) or 1000 (Condé et al., 2007),
224 corresponding to a hard ground (Beltrami et al., 1994; Condé et al., 2007). It is interpreted as
225 resulting from regional flooding affecting the basin during the lower Aptian (Pessoa Neto et
226 al., 2004).

227 The transitional sequence (Paracuru Fm.) marks by the first marine incursions
228 affecting the Mundaú sub-basin, alternating within fluvial, deltaic and lacustrine sandstones.
229 Limestones and subordinate evaporites were also deposited at this stage (Costa et al., 1990;
230 Beltrami et al., 1994; Condé et al., 2007) (Fig. 2). As shown by Maia de Almeida et al. (2020),
231 the Paracuru Formation represents a *breakup sequence* sensu Soares et al. (2012) and Alves
232 and Cunha (2018).

233 The drift or marine megasequence, developed in association with continental drift
234 between the BEM and Equatorial Africa, reflects a prolonged phase of thermal subsidence. The
235 resulting drift strata in the Ubarana Formation comprises two members (Costa et al., 1990;

236 Beltrami et al., 1994; Condé et al., 2007) (Fig. 2). The first of these two members, the
237 Uruburetama Member, corresponds to a marine transgression and consists chiefly of shales.
238 The second member, the Itapagé Member, corresponds to a regressive marine phase and
239 consists of turbiditic shales and sandstones (Costa et al., 1990; Beltrami et al., 1994; Condé et
240 al., 2007). The Guamaré Formation consists of shelf carbonates, while the Tibau Formation
241 comprises proximal sandstones. The clastic continental sediments of the Barreiras Formation
242 comprise the youngest unit in the basin (Condé et al., 2007) (Fig. 2).
243
244
245 **2.3. Curimã and Espada fields**
246
247 The Curimã field is a classic example of a combined hydrocarbon trap resulting
248 from the erosional truncation of large, active tilt blocks. The combined trap is made up of
249 rotated blocks composed of Aptian strata that are truncated at the top by an angular
250 unconformity, therefore juxtaposing Aptian reservoirs and Albian-Turonian transgressive
251 shales (Pessoa Neto, 2004). The main reservoirs in the Curimã field comprise fluvial and
252 deltaic sandstones with good permeability and porosity characteristics, which are laterally
253 continuous in the Mundaú and Paracuru Formations. Porosity varies from 15.6% to 22.3% in
254 the Paracuru Formation and 18.4% to 27.7% in the Mundaú Formation, while permeability
255 varies from 27.4 mD to 401.6 mD in the Paracuru Formation and from 65.2 mD to 212.8 mD
256 in the Mundaú Formation (ANP, 2016). Reservoirs in the Paracuru Formation are filled with
257 31° API oil, whereas the Mundaú reservoirs contain 29°API oil. In the Paracuru Formation, the
258 primary mechanism of production is gas in solution. In addition, water injection has been
259 applied since 1985 with the aim of enhancing oil recovery.

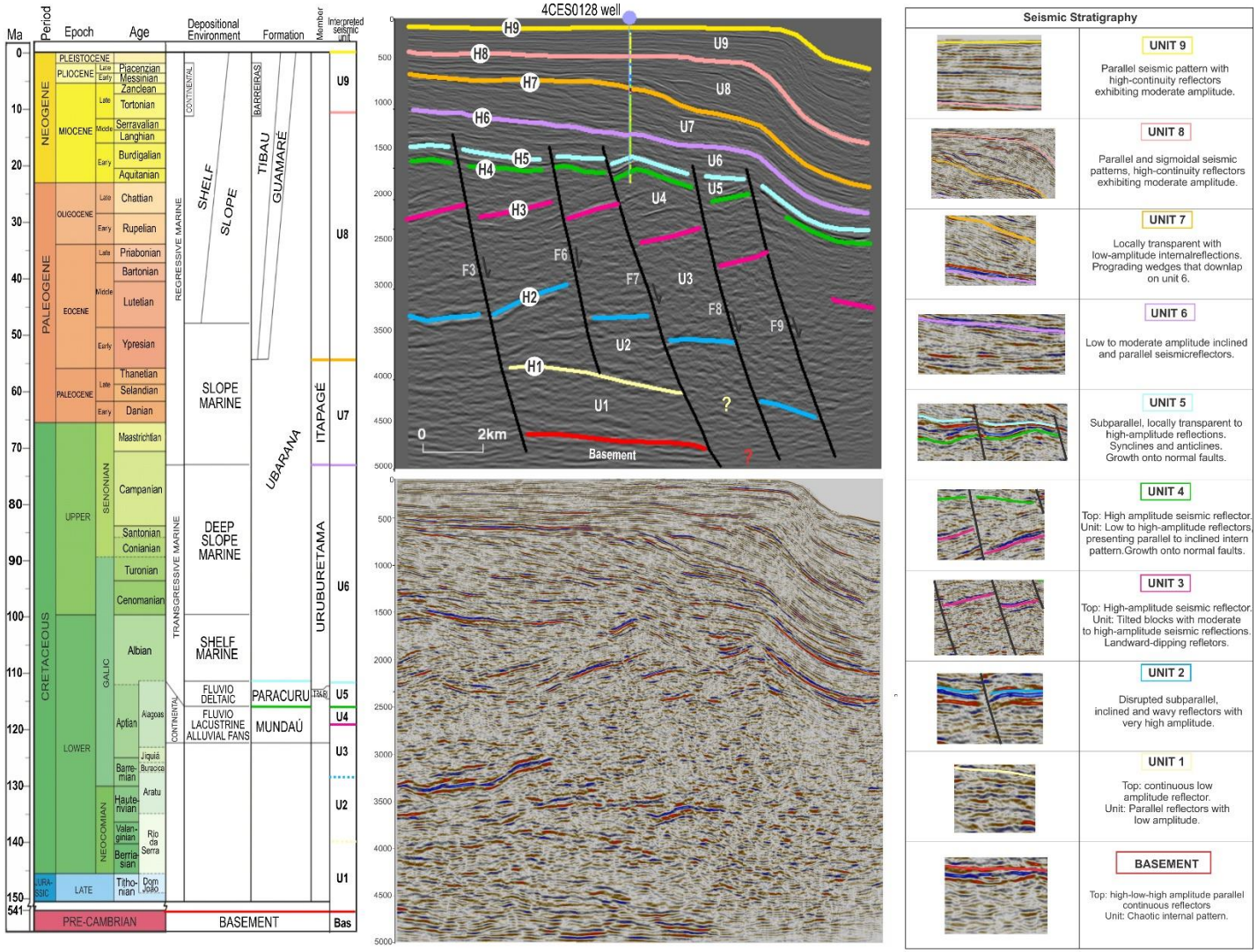

Figure 2. Correlation panel amongst interpreted seismic units and stratigraphic information from the Ceará Basin (Condé *et al*., 2007). See location of the seismic section in Figure 1.

In the Mundaú Formation, the primary mechanism of production is combined water inflow due to an adjacent aquifer and resulting expansion of a gas cap (ANP, 2016).

The main reservoirs in the Espada field are located in a turbiditic play comprising sandstones intercalated to shales of Ubarana Formation (Costa et al., 1990). The reservoirs are filled with 37° API oil (ANP, 2017a). The main producer zone is approximately 10 m thick, porosity varies from 24.5% to 32.3%, and permeability varies from 200 mD to 9000 mD (ANP, 2013).

3. MATERIAL AND METHODS

Data from 12 exploration wells and a post-stack time-migrated multichannel three-dimensional seismic reflection volume in the time domain (0223_CURIMA_ESPADA_4A.3D. MIG_FIN) were used in this study (Fig. 1). The interpreted seismic volume consists of 171 inlines spaced 75 m (IN95 - IN266) with a 35°azimuth, and 662 crosslines (XL77 - XL739) spaced 25 m with a 125°azimuth. It covers part of Espada field and the entire Curimã field, spanning the mid continental shelf, the outer continental shelf and the upper continental slope (Fig. 1). The inline length is ~16.6 km and crosslines are ~12.8 km long, reaching a total area of ~212 km². Penetration depth reaches 5,000 ms two-way time (twt) and each seismic trace has 1,251 samples at a 4 ms sampling interval. The 3D post-stack seismic data was supplied with a standard processing flow (migrated post-stack).

The interpreted well data include standard log suites (i.e. gamma ray, sonic, density and resistivity), lithological data and formation tops. Some wells (e.g. 4CES0128, 4CES0143

and 1CES0115) display check-shot surveys. All these data were acquired by Petrobras and supplied by the Brazilian National Agency of oil, gas and biofuels (ANP).

Well and seismic data integration was performed on Schlumberger's Petrel E&P Software Platform. The interpretation of the seismic data (horizons and faults) was performed in the time domain. Thus, we converted the well data into the time domain using the check-shots and sonic logs (Fig. 3). We produced a synthetic seismogram and correlated it to the real seismic data. Seismic interpretation was based on the general principles of seismic stratigraphy (Mitchum et al., 1977), which rely on the recognition of seismic patterns such as seismic terminations, seismic facies and seismic units. First, we interpreted the main seismic horizons and faults in the Mundaú sub-basin. In a second stage, we created fault polygons and their boundaries. Finally, the horizons and faults interpretations were used to generate surfaces and then to extract the thickness maps (Fig. 3).

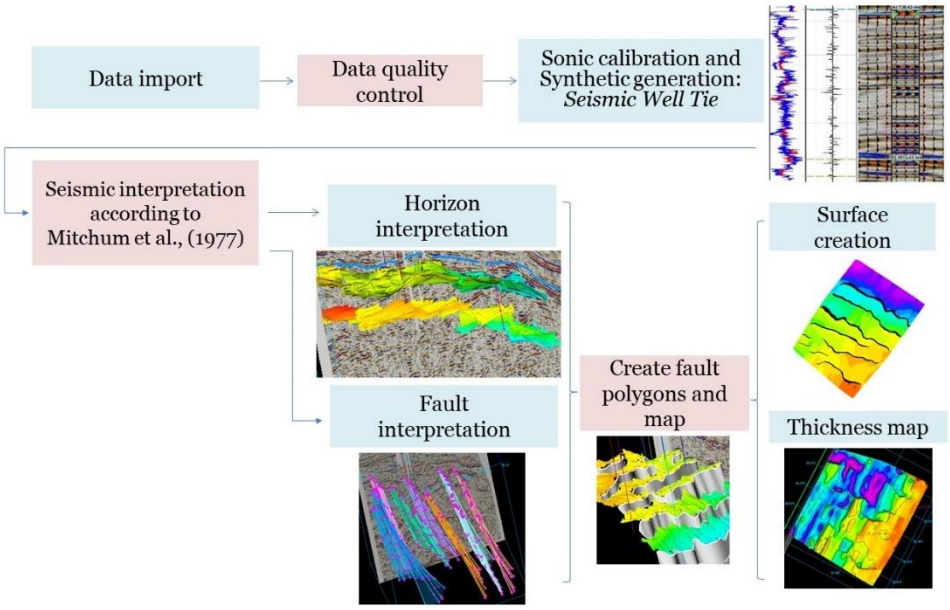

Figure 3. Flow chart summarising the methodology used in this work.

4. RESULTS

306 **4.1 Seismic Stratigraphy**

307

308 Nine seismic sequences were interpreted and correlated with the regional
309 lithostratigraphic framework of Condé et al. (2007) (Figs. 2 and 4). Units 1, 2, 3 and 4 comprise
310 the syn-rift Mundaú Formation.

311 The **top basement** reflection was mapped in the central part of the study area (Figs.
312 5j and 6). In the study area, basement rocks are characterised by their chaotic internal pattern,
313 with the top of this unit comprising a continuous reflection of variable amplitude (Fig. 2). The
314 top basement reflection generally dips to the NNW at an angle varying from 0° to 72°, with an
315 average dip of 15°.

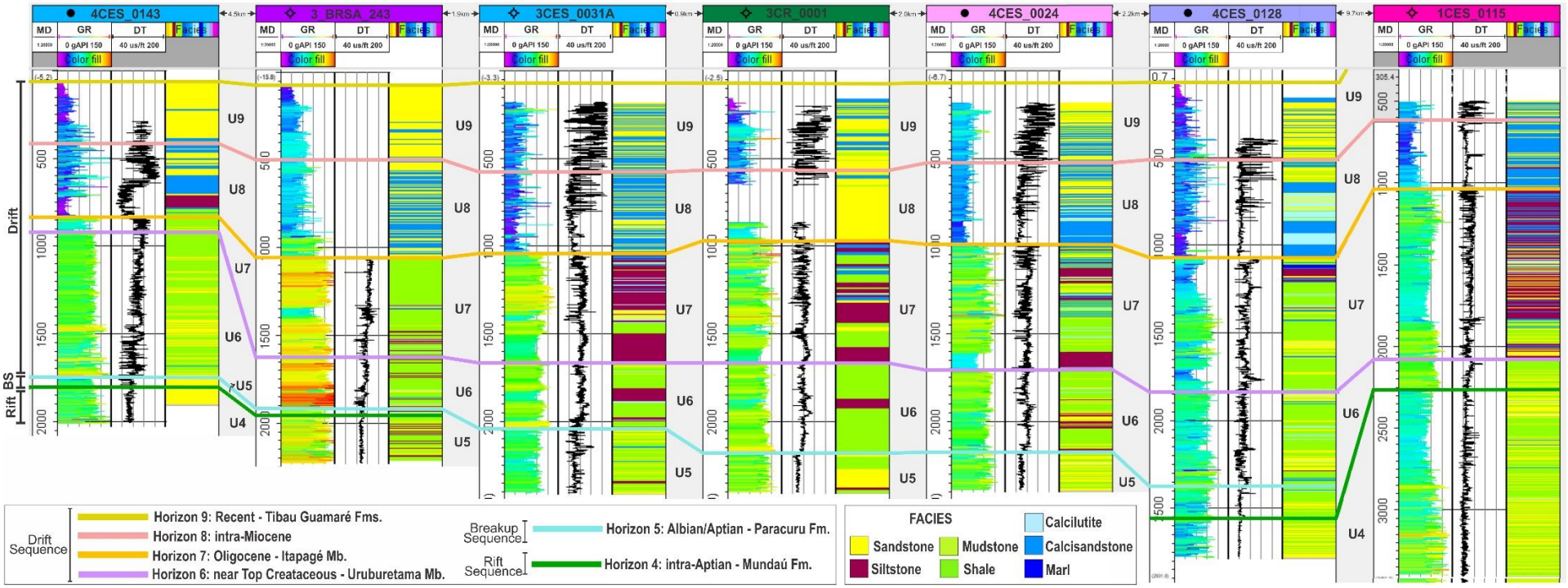

Figure 4. Well correlation panel showing interpreted seismic units, gamma ray, sonic logs and facies, highlighting the sequences: rift, transitional (breakup sequence - BS) and drift.

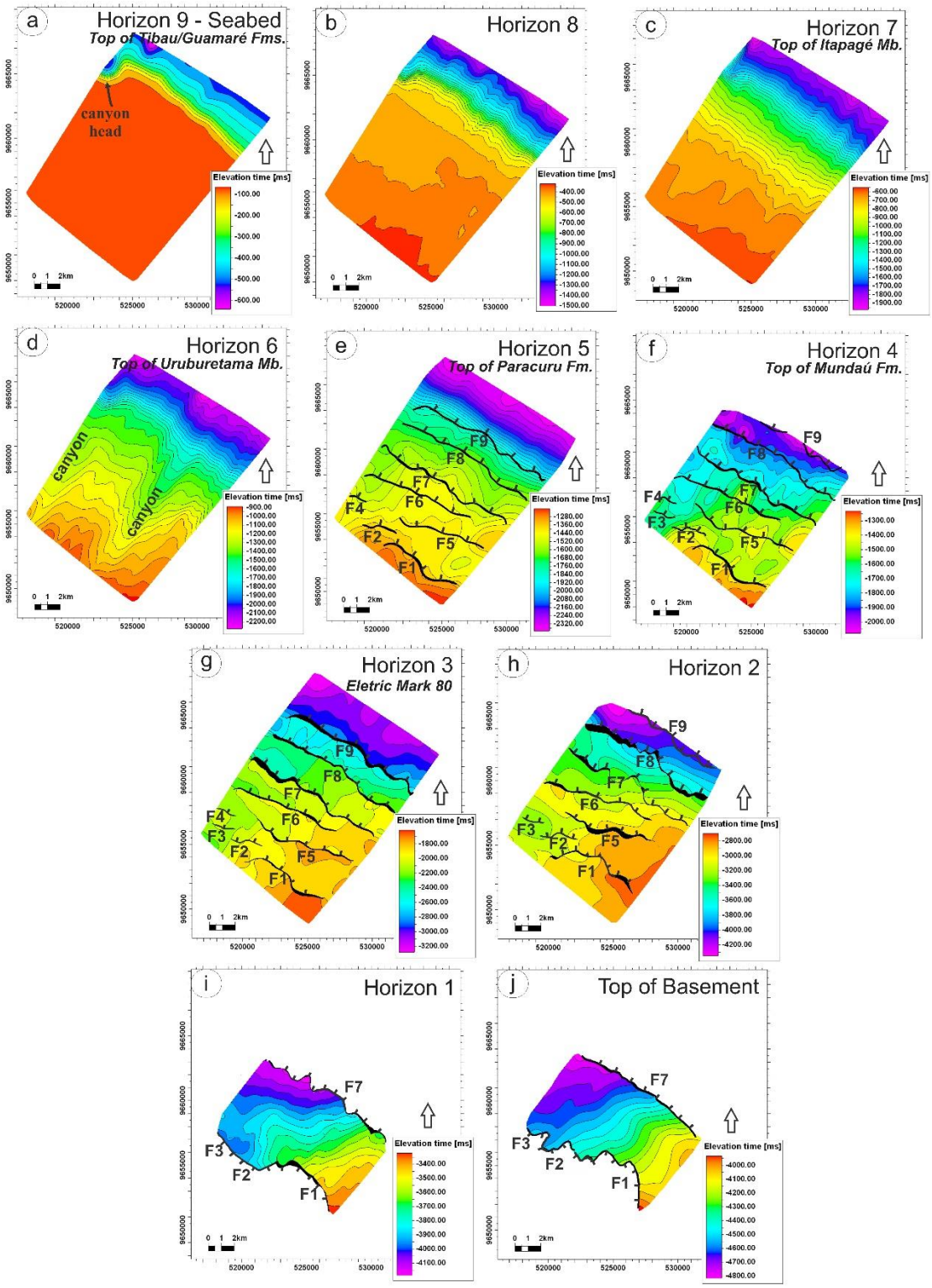

Figure 5. Time-structural maps of various horizons at the study area: A) Sea floor (Top of the Tibau and Guamaré Formations) revealing submarine canyons in the shelf-edge region and on the continental slope. B) Horizon 8. C) Horizon 7 (Itapagé Member). D) Horizon 6, which corresponds to the top of the Uruburetama Member. Two submarine canyons incised the continental slope at this stage. E) Horizon 5 (Top of the Paracuru Formation) revealing the reactivation of faults during the transitional phase. F) Horizon 4, correlating with the top to the Mundaú Formation. This horizon was offset the syn-rift faults. G) Mark 80 horizon (top of Unit 3). H) Horizon 2 showing a faulted surface with a structural high to the SSE. I) Top of Unit 1 (Horizon 1) as mapped in the central part of the study area. J) Top of Basement mapped in the central part of the study area.

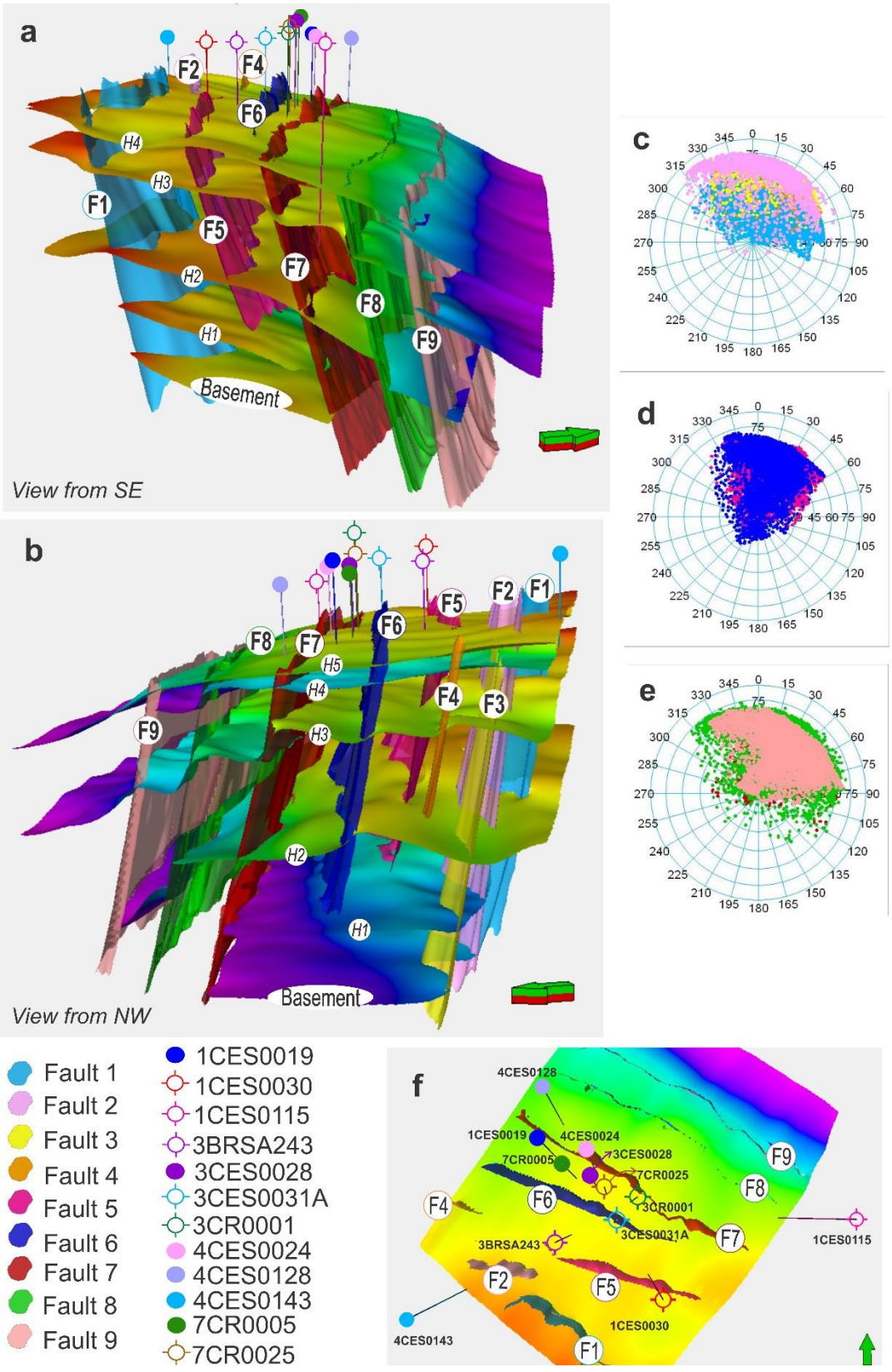

Figure 6. A) and B) 3D structural models of the study area with view from southeast and northwest, respectively. C) Stereoplot of interpreted fault planes (as interpreted on seismic) showing the dip angle and dip azimuth of Faults 1, 2, 3 and 4. D) Corresponding stereoplot for Faults 5 and 6. E) Corresponding stereoplot for Faults 7, 8 and 9. F) Map view from above showing interpreted faults 1 to 9 and exploration wells.

334 **Unit 1** is characterised by its parallel internal reflections with low amplitude,
335 similarly to the basement, and was clearly mapped in the central part of the study area (Figs. 5i
336 and 6). The top of Unit 1 (Horizon 1) is a continuous low-amplitude reflection (Fig. 2).
337 The top reflection in **Unit 2** is a faulted, high-amplitude horizon that occurs at a
338 depth of ~ 3,000 ms two-way time (Horizon 2). Unit 2 is characterised by its sub-parallel,
339 inclined and wavy internal reflections with very high amplitude (Fig. 2). A basement high
340 affects the unit in the SSE part of the study area, where internal reflections dip to the NNW
341 (Fig. 5h). Units 1 and 2 were not crossed by exploration wells.
342 The top of **Unit 3** (Horizon 3) is correlated with the Electric Mark 80 (Costa et al.,
343 1990) or 800 (Condé et al., 2007). In the study area, it is a high-amplitude seismic reflection
344 with poor continuity (Fig. 2). Horizon 3 is a key to the mapping of faults in the study area when
345 considered together with Horizon 2. Unit 3 shows moderate to high-amplitude seismic
346 reflections tilted by normal faults. These reflections can be landward-dipping in places. Unit 3
347 is composed of intercalated shales and sandstones (Fig. 4), showing strata growth in the
348 immediate footwall of normal faults (Fig. 7d). It reaches a maximum thickness of 1,750 ms.

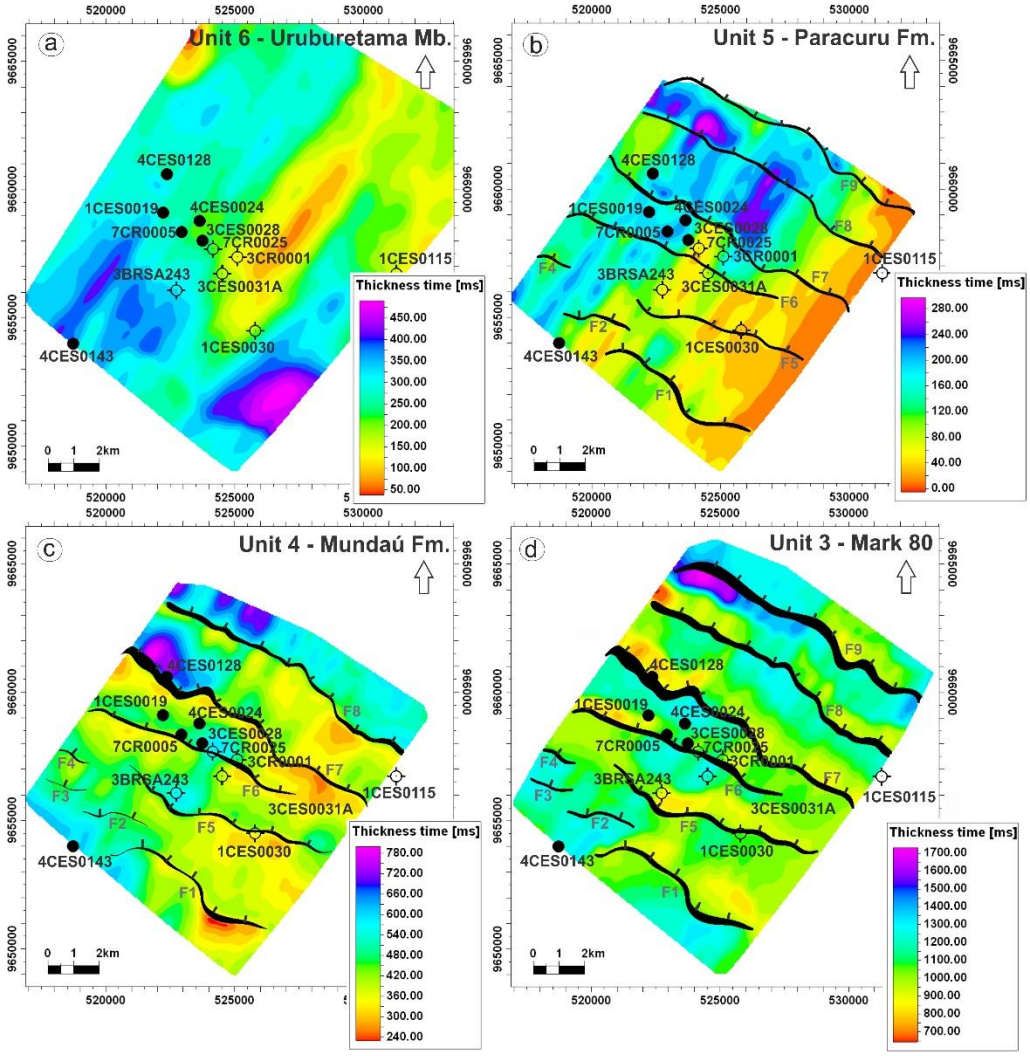

Figure 7. Isochron thickness of: A) Unit 6 (Uruburetama Member). In the central part of the study area, there is a region with smaller thickness - see orange color. B) Unit 5 (Paracuru Formation). Widespread erosion removed the upper part of this formation reducing its thickness in the south and southeast of the study area. C) Unit 4, corresponding to the upper part of the Mundaú Formation. This map shows the sedimentary thickening on the downthrown side of the faults, revealing fault activity. D) Unit 3, showing an increase in thickness as one gets closer to the upthrown side of normal faults.

Unit 4 comprises low- to high-amplitude internal reflections that are sub-parallel to gently dipping. It is composed of sandstones, siltstones and shales (Figs. 2 and 4). The upper boundary of this unit (Horizon 4) coincides with the high-amplitude Electric Mark 100 (Costa et al., 1990) or 1000 (Condé et al., 2007). Unit 4 fills multiple half-grabens where it shows growth onto active faults, thus reflecting the development of a syn-rift sequence. In contrast to Unit 3, Unit 4 presents thicker strata on the downthrown side (immediate hanging-wall) of faults (Fig. 7c). All imaged faults intersect Unit 4 in its entirety (Figs. 5f and 6).

364 **Unit 5** comprises subparallel, locally transparent to high-amplitude seismic
365 reflections, part of the Paracuru Formation. It is composed of thin intercalations of sandstone,
366 siltstone, shales and marls (Figs. 2 and 4). Unit 5 is a transitional unit, a *breakup sequence*
367 sensu Soares et al. (2012) and caps the half-grabens associated with syn-rift faults. Its top
368 (Horizon 5) is an angular unconformity; widespread erosion removed the upper part of this unit
369 (Fig. 7b). As a result, Unit 5 becomes thinner in the east and southeast parts of the study area.
370 In the eastern part, close to the 1CES0115 well, Unit 5 was totally eroded. Units 4 and 5 present
371 growth onto major normal faults, highlighting active tectonic subsidence during their
372 accumulation.

373 **Unit 6** was deposited during the drift phase. However, faults still offset its lower
374 part. Unit 6 displays low- to moderate-amplitude inclined reflections comprising calcareous
375 shales with sandstones and siltstones intercalations (Fig. 4). Marls and calcilutites were drilled
376 in some wells. Unit 6 comprises the Uruburetama Member of the Ubarana Formation (Fig. 2)
377 and its top (Horizon 6) corresponds to an erosional surface associated with the incision of two
378 submarine canyons. The Espada and Curimã fields are located between these two submarine
379 canyons (Figs. 5d and 7a).

380 The upper boundary of **Unit 7** (Horizon 7) is a low-amplitude continuous
381 reflection. Unit 7 is locally transparent with low-amplitude internal reflections (Fig. 2). Internal
382 reflections in Unit 7 reveal prograding wedges of strata that downlap onto Unit 6. Unit 7
383 comprises the regressive Itapajé Member of the Ubarana Formation. Lithologically, it is
384 composed of intercalations of sandstones, siltstone, marls, calcilutites and shales (Fig. 4).

385 **Unit 8** reveals parallel and sigmoidal seismic reflections with high continuity and
386 moderate amplitude (Fig. 2). Lithologically, Unit 8 is composed of calcarenites, calcilutites,
387 sandstones and shales (Fig. 4).

388 **Unit 9** consists of parallel seismic reflections with high continuity and moderate
389 amplitude (Fig. 2). It is mainly composed of sandstones and calcarenites with thin layers of
390 shales. In the northern region of the study area, there is a submarine canyon head incising the
391 continental shelf edge (Fig. 5a). Units 8 and 9 comprise the Tibau and Guamaré Formations.
392
393 **4.2 Tectonic framework**
394
395 The study area presents a synthetic fault arrangement to the main extensional fault
396 bounding the Mundaú sub-basin (Mundaú Fault). In general, normal faults are seaward-dipping
397 and strike to the NW, dipping to the northeast. The faults are planar at depth (Figs. 2 and 6).
398 In the mid continental shelf, Faults 1, 2, 3 and 4 display an *en echelon* geometry
399 (Figs. 5j and 6) and, except for Fault 4, they all offset basement units. Faults 2, 3 and 4 are
400 respectively 2.7, 1.7 and 1.3 km long, being the smallest faults in the study area. They are
401 closely spaced with an average spacing of around 1 km, and with relatively rectilinear traces.
402 This is chiefly the case for Faults 3 and 4 (Figs. 5 and 6).
403 Faults 5 and 6 present sinuous traces and offset Units 2 to 6, tipping out near the
404 top of Unit 1 (Fig. 6). Faults are up to 9 km long and dip to the NNE with and average angle
405 of 41° (Fig. 5).
406 On the outer shelf, the high-angle Faults 7, 8 and 9 are the longest in the study area
407 (~11 km), occurring along the entire seismic volume. Fault 7 is located 2.7 km away from Fault
408 8, while this latter is spaced 1.9 km from Fault 9. All these faults are parallel and sinuous. In
409 addition, they are responsible for the largest offsets observed in the study area.
410
411
412

4.3 Well data from the Curimã and Espada fields

After completing detailed seismic and structural interpretations, one can understand that wells 1CES0019, 4CES0024, 3CES0028 and 7CR0005 were drilled between Faults 6 and 7, successfully striking oil in the Curimã field (Table 1, Figs. 6 and 7). Wells 3CR0001 and 7CR0025 were also drilled between Faults 6 and 7, but did not find any hydrocarbons.

437 Table 1. Integrated compilation of data from exploratory wells and seismic interpretation, showing the well location between the interpreted faults, oil field, category,
438 objective, classification and oil finds.
439

Well	Between the faults	Oil field	Year	Category	Objective	Classification	Oil finds
1CES0019	6 e 7	Curimã	1978	Pioneer	Testing the dome structure next to Paracuru top.Targets: reservoirs of Paracuru and Mundaú Fms.	Discoverer of oil field	Units 5 and 6
4CES0024	6 e 7	Curimã	1978	Adjacent pioneer	Main objective: sandstones of Paracuru Fm. equivalent to 1CES0019 producer. Secundary objective: Turbiditic sandstones of Ubarana Fm.	Subcomercial oil producer	Units 4, 5 and 6
3CES0028	6 e 7	Curimã	1978	Extension	Verifying the SE extension of oil accumulation of Curimã field	Oil producer	Unit 5
7CR0005	6 e 7	Curimã		Exploratory	Knowing reservoir parameters and static pressure level	Comercial oil producer	Unit 5
4CES0128	7 e 8	Curimã	1996	Adjacent pioneer	Testing the dome structure next to Paracuru top	Discoverer of new oil area	Units 4, 5 and 6
3CR0001	6 e 7	Curimã	1979	Extension	Verifying the SE extension of oil accumulation of Curimã field	Dry with oil shows	-
7CR00025	6 e 7	Curimã	1989	Exploratory	Knowing reservoir parameters and static pressure level	Dry with oil shows	-
3CES0031A	5 e 6	Curimã	1979	Extension	Verifying the SE extension of oil accumulation of Curimã field	Dry	-
3BRSA243	5 e 6	Curimã	2003	Extension	Verifying the S extension of oil accumulation of Curimã field	Dry	-
1CES0030	5 e 6	-	1979	Pioneer	Testing tilted block formed by the fault 5	Dry	-
1CES0115	7 e 8	-	1991	Pioneer	Testing tilted block structured between the faults 7 and 8	Dry with oil shows	-
4CES0143	2	Espada	1998	Adjacent pioneer	Turbiditic sandstones of Ubarana Fm.	Subcomercial oil producer	Unit 6

Well 4CES0128, drilled between Faults 7 and 8, found new reservoir intervals in the study area (Table 1, Fig. 8a). Fault activity resulted in the formation of an anticlinal trap near Unit 5, i.e. in the Paracuru Formation. Well 4CES0128 found oil in Units 4, 5 and 6 (Ubarana, Paracuru and Mundaú Formations).

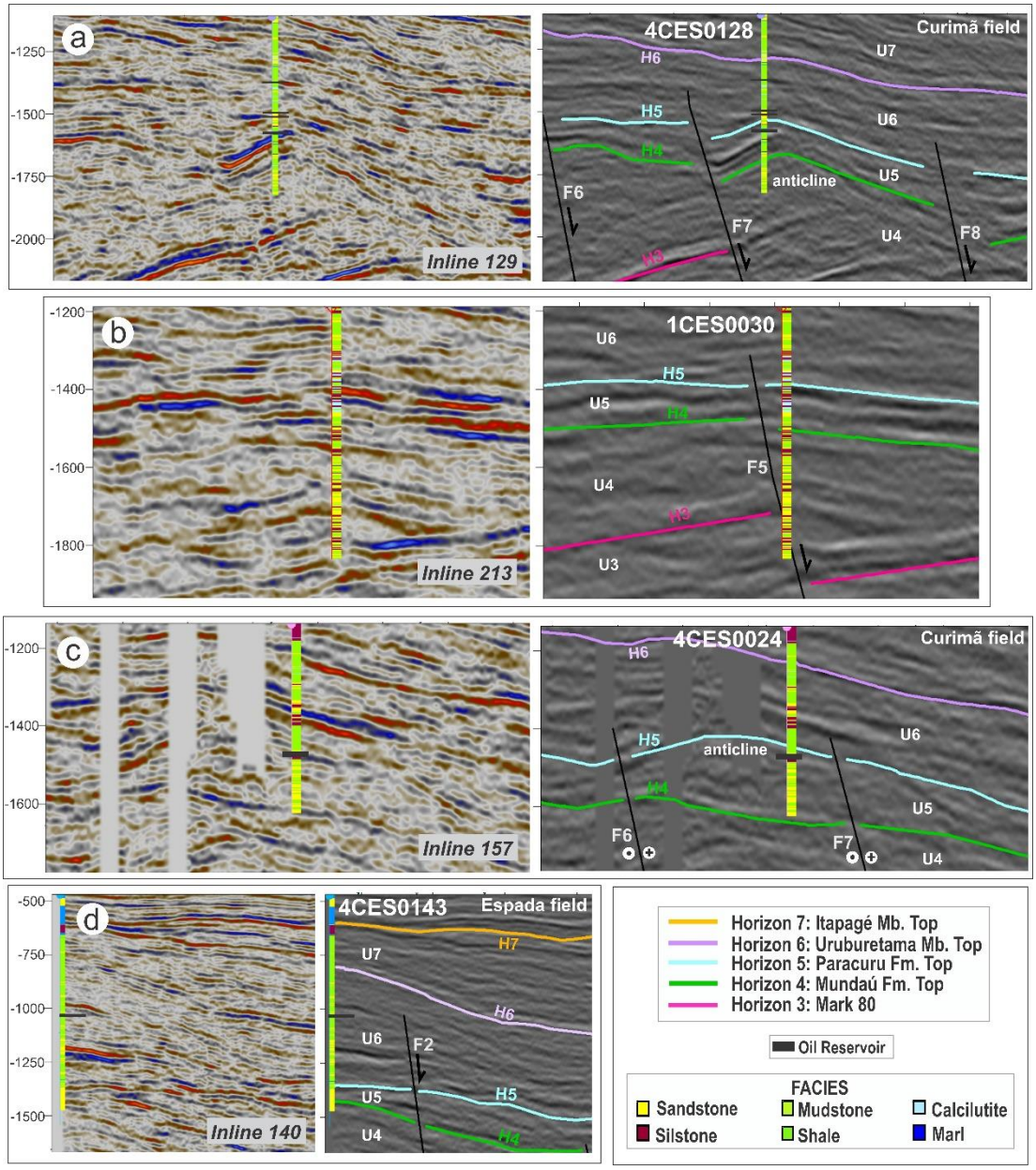

Figure 8. SW-NE seismic section interpreted with faults, horizons and wells, highlighting the seismic units. A) Well 4CES0128 reached the Unit 4 (Mundaú Fm.) and drilling oil reservoirs in stratigraphic (turbiditic) and structural (anticline) plays. B) Well 1CES0030 drilled in the fault zone (downthrown side of Fault 5). C) Well 4CES0024 drilled on the footwall of the Curimã Fault (Fault 7). Anticline structure on the tilt-block formed between Faults 6 and 7 at the level of the Unit 5 (Paracuru Formation). This anticline shows an accumulation of oil in place. D) Well 4CES0143 crossing the Espada field and corresponding turbiditic reservoir successions in the Unit 6 (Ubarana Formation).

In the eastern part of the area, where the basement is shallow and Unit 5 was eroded, well 1CES0115 was drilled with the aim of testing the half-graben delimited by Faults 7 and 8 (Fig. 7). The aim of this well was to reach fluvio-deltaic sandstones in Units 3 and 4 (Figs. 4 and 6). However, the well revealed reduced net pays, an undefined oil water contact, low transmissibility and very low productivity. The section below Horizon 3 showed very poor reservoir quality with a marked reduction in porosity with depth – a character further worsening the quality of the reservoirs drilled at this location. The well was classified as 'dry with hydrocarbon shows' and was abandoned.

Well 3CES0031A was drilled on top of the footwall bounded by Fault 6. This and well 3BRSA243 were drilled between Faults 5 and 6 with the aim of verifying the SE extension of the Curimã field (Figs. 6 and 7, Table 1). They did not find any hydrocarbons and were considered dry.

Well 1CES0030 was drilled exactly at Fault 5, reaching the lower part of the block limited by Faults 5 and 6, i.e. the immediate hanging-wall of Fault 5 (Fig. 8b). Well data show clayey sandstones, water saturation and low permeability. The well was eventually abandoned due to the lack of economic volumes of hydrocarbons. Well 1CES0143, in the southwest portion of the study area, is located at the Espada field (Table 1, Figs. 1 and 6). It detected oil shows in Units 5 and 6 and is, at present, an oil producer within the Ubarana Formation. Well tests developed in the interval spanning 1,263-1,278 m produced 26°API oil with a flow of 80 m^3/day (Fig. 8d).

5. DISCUSSION

5.1 3D Structural modelling of an oil producing region of the BEM

Our 3D structural modelling suggests that the study area, comprising an oblique rift basin with multiple half-grabens, records active faulting during the deposition of Units 1 to 4 (syn-rift). Figs. 7c and 7d show that important fault activity occurred during the deposition of Unit 4 (Aptian). These faults were capable of tilting the blocks where Units 2 and 3 were deposited (Fig. 7d), resulting in the thickening of Unit 4 next to fault planes (growth faults) (Fig. 7c). These observations corroborate the published literature and confirm that the continental margins along the Equatorial Rift Segment (EqRS) were affected by a paroxysmal phase of tectonism between South America and Africa during the Aptian, with a major phase of rift-related subsidence being reported from all EqRS basins (Azevedo, 1991; Brownfield and Charpentier, 2006; Soares Junior et al., 2011; Heine and Brune, 2014).

Near the Xaréu Oil Field (Fig. 1), Antunes et al. (2008) mapped an array of NW-trending and NE-dipping normal faults forming an extensional system that is very similar to the study area in this work. However, faults in the Xaréu field are listric and rooted along a detachment surface corresponding to the Mundaú Fault, located at the southwest border of the Mundaú sub-basin. In addition, Antunes et al. (2008) interpreted these faults as representing listric or ramp-flat-ramp geometries. According to the interpretations in this work, faults are planar and sub-vertical in the Curimã field, forming tilt blocks. This compares favourably with basins on the BEM (Watts et al., 2009; Zalán, 2015) and Equatorial Africa (Tetteh, 2016) such as in the Guyana–Suriname (Nemčok et al., 2016a; Nemčok et al., 2016b), in which syn-rift planar faults were also recognised.

During the deposition of Unit 5 (transitional unit), faults continued to be active as transtensional structures, forming folds between active faults (Figs. 8a, 8c, 9e and 9f). The top of Unit 5 is an erosional unconformity recognised in the western portion of the Equatorial South America (Nemčok et al., 2016a), as well as in Equatorial Africa (Brownfield and Charpentier, 2006), and has been interpreted as a breakup unconformity. The exact location along the EqRS

where continental breaup was occurring at the time, or if this stratigraphic surface represents full lithospheric or mantle breakup, is still under debate (see Soares et al. 2012; Alves and Cunha, 2018 and Maia de Almeida et al., 2020). Similarly to the study area, Nemčok et al. (2016a and 2016c) show evidence for folding of strata near the breakup unconformity before late Aptian–Albian times. They noted the presence of the breakup unconformity on top of a folded section characterised by significant erosion of the Demerara Plateau. In parallel, Attoh et al. (2004) confirmed this same episode of subaerial erosion offshore Ghana and attributed lateral variations in erosional depth to crustal displacement associated with local folding and uplift.

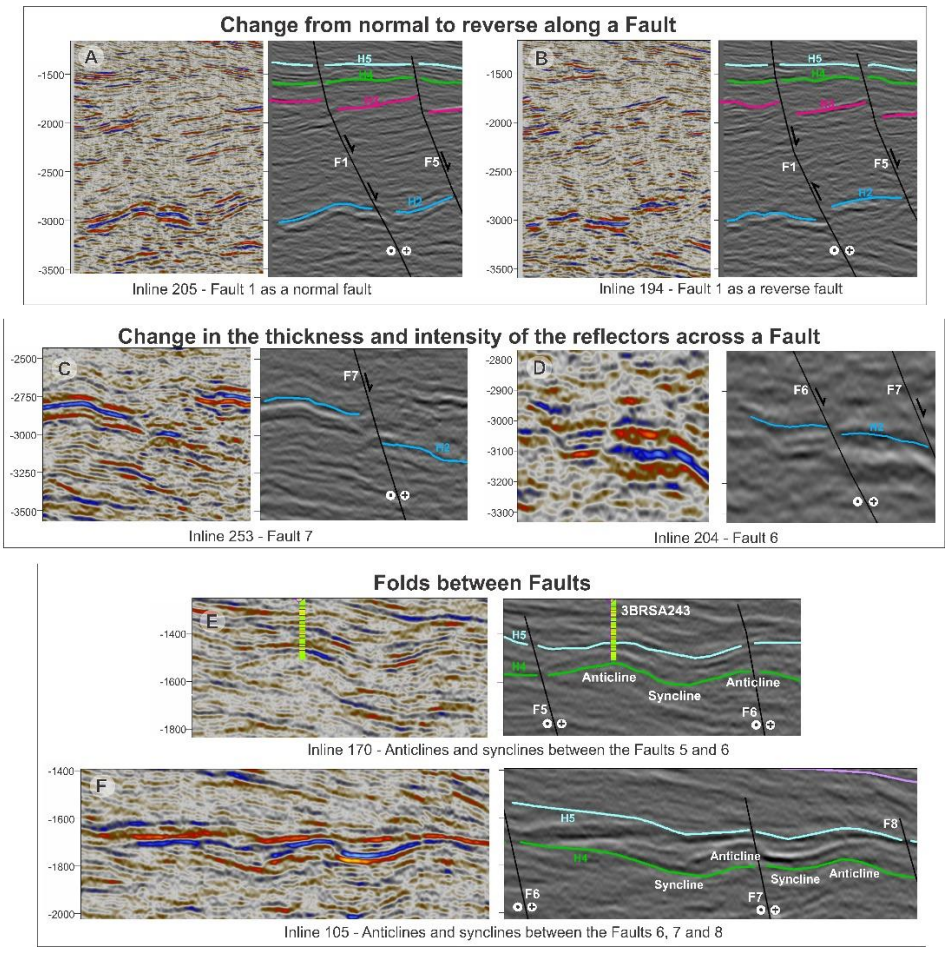

Figure 9. Seismic patterns of strike-slip tectonics. A) Variations of fault throw with depth (Fault 1). B) Change from normal to reverse fault movement with depth (Fault 1). C) Abrupt change in the seismic character of the reflector across Fault 7. D) Abrupt change in the seismic character of the reflector across Fault 6. E) Synclines and anticlines in the breakup sequence (Unit 5) between the faults 5 and 6. F) Synclines and anticlines in the breakup sequence (Unit 5) between the faults 6, 7 and 8.

519 The development of folds in extensional basins is not common. However, fault-related
520 folds have been recognised close to propagating normal faults (Brandes and Tanner, 2014) as
521 observed in the study area (Figs. 8 and 9). Fault-related folding has been analysed in the field
522 (Howard and John, 1997; Corfield and Sharp, 2000; Sharp et al., 2000), using analogue models
523 (Withjack et al., 1990), and numerical simulations (Khalil and McClay, 2002; Jin and
524 Groshong, 2006). Analogue models developed by McClay and Scott (1991) reveal that small
525 irregularities in the geometry of normal faults can generate reverse secondary faults and local
526 antiforms within a general setting dominated by regional extension. These antiforms are similar
527 to the structure drilled by well 4CES0128 (Fig. 8a).
528 Folds generated between normal faults can be also associated to strike-slip tectonics
529 (Zalán, 1986; Lamarche et al., 1997; Davison et al., 2016). According to Fossen et al. (2013)
530 and Fossen (2016), transcurrent faults zones can develop folds; folds are arranged spatially
531 such that culminations and depressions in successive folds lie along lines that make an acute
532 angle with the (approximately parallel) fold axes. Such folds are stepped, and, in general,
533 arranged in an *en echelon* geometry. In the study area, folds are relatively sub-parallel to faults,
534 showing very acute angles. In addition, folds were mapped in other regions of the BEM such
535 as in Barreirinhas and Pará-Maranhão basins by Azevedo (1991) and Sauerbronn (1996), in the
536 Piauí-Camocim sub-basin by Zalán & Warme (1985), in Icaraí sub-basin by Castro (1993), in
537 Potiguar Basin by Hoerlle et al. (2007), in the Guyanas-Suriname basins by Goss et al. (2008),
538 Nemčok et al. (2016a) and Loncke et al. (2016) and in Equatorial Africa by Attoh et al. (2004),
539 Lamarche et al. (1997) and Davison et al. (2016).
540 he *en echelon* geometry of normal faults observed in the study area is a common fault
541 geometry in transcurrent structures (Hempton and Neher, 1986; Deng et al., 1986; Lonsdale,
542 1989; Moustafa and Abd-Allah, 1992; Zachariasen and Sieh, 1995) (Figs. 5 and 7). Hence,
543 using the criteria of Zalán (1986), other characteristics revealing strike-slip movements were

544 investigated in the study area, such as the sinuous and complex geometries of fault planes and
545 profiles (Figs. 6 and 7). High sinuosity in faults is an important trait of transcurrent faults
546 (Bridwell, 1975). Moreover, Fault 1 changes from normal to reverse along its strike (Figs. 9a
547 and 9b). In Fig. 9a, Horizons 2 and 3 are subtly displaced by Fault 1. However, in Fig. 9b, Fault
548 1 displaced Horizon 2 as a reverse fault and Horizon 3 as a normal fault. Apart from changing
549 from normal to reverse fault along strike, this fault also reveals important changes in throw
550 with depth, two characteristics associated with strike-slip movements (Zalán, 1986). Offshore
551 Ghana, Attoh et al. (2004) also mapped contradictory offsets that indicate strike-slip tectonics.
552 Variations in the seismic character across a fault were also interpreted as relating
553 to strike-slip movements. Seismic facies reveal changes in thickness and intensity of the
554 seismic reflections, and relative scale of deformation in strata (Figs. 9c and 9d), corroborating
555 the idea that strike-slip tectonics affected great part of the study area. Similarly, Andrade *et al.*
556 (2018) interpreted changes in the seismic reflections close to the Romanche Fracture Zone as
557 revealing a dense set of strike-slip faults. Such interpretations have important economic
558 implications because it increases the variability of potential traps around the Romanche
559 Fracture Zone (Zalán, 1986).
560 Ultimately, the 3D structural model presented in this work is a combination of the
561 geometries 1 and 3 proposed by Matos et al. (1996) (*see item 2.1.1 Mundaú sub-basin*).
562 Therefore, we propose a fourth complementary geometry that includes tilted blocks with small
563 anticlines and synclines genetically related to transtensional planar faults. This model fits
564 within the regional context of oblique rifting in the Brazilian Equatorial Margin.
565
566 *5.2 Petroleum plays in the Curimã and Espada Fields: Comparison with other Equatorial*
567 *Atlantic plays*
568

569 Three types of petroleum plays were found in the study area: combined, structural and
570 stratigraphic (Fig. 10). They are described as follows:
571
572 *5.2.1. Combined plays*
573 Pessoa Neto (2004) summarised the essential conditions to form combined traps in the
574 Curimã field: large-slip faults and the presence of angular unconformities followed by the
575 deposition of thick transgressive marine shales. In addition, three geological settings were
576 considered by Pessoa Neto (2004) to record some degree of inefficiency in hydrocarbon traps:
577 1. juxtaposition of reservoir intervals and sandy layers across fault planes or unconformities;
578 2. the absence of erosional truncation in tilt blocks and; 3. erosion or non-deposition of
579 transgressive marine strata above reservoir intervals.
580 Based on our 3D structural model, Faults 6 and 7 are key to understand the
581 petroleum potential of the Mundaú sub-basin - wells 1CES0019, 4CES0024, 3CES0028 and
582 7CR0005 drilled between these two faults and found oil in the Curimã field (Table 1, Figs. 7,
583 8 and 10). These wells drilled key examples of the **combined plays** proposed by Pessoa Neto
584 (2004). Wells 1CES0019 and 4CES0024 reached a dome structure formed by Faults 6 and 7
585 and reached the upthrown side (footwall) of a mixed trap formed by the block tilted by Fault 7
586 and the shales deposited above Horizon 5 (Figs. 8c and 10). The upthrown sides of normal
587 faults, forming tilt blocks, are classic footwall traps for hydrocarbon (Illing and Hobson, 1981;
588 Brooks and Glennie, 1987; Yielding, 1990; Hardman and Booth, 1991; Nemčok, 2016d).
589 According to Pessoa Neto (2004), Aptian reservoirs are located on the footwall of the main
590 fault bounding the Curimã field, i.e. the Curimã Fault. Thus, we can deduce that Fault 7 is the
591 Curimã Fault proposed by Pessoa Neto (2004).
592

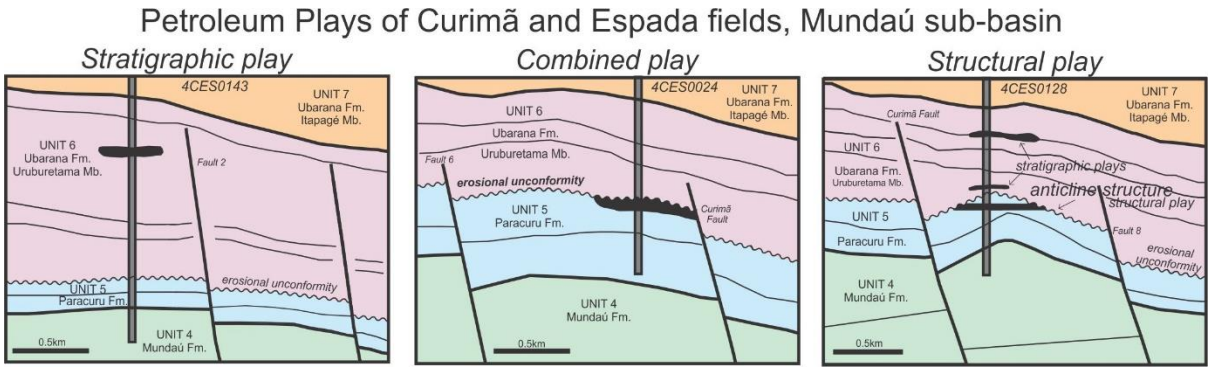

Figure 10. Three types of petroleum plays in the Curimã and Espada fields, Mundaú sub-basin: stratigraphic, combined and structural plays.

The Curimã field is delimited to the north by the Curimã Fault (Fault 7), which affects Units 4 and 5 (Paracuru and Mundaú Formations). However, Fault 7 also offsets the lower part of Unit 6 (Uruburetama Member). To the south, the field is delimited by a synthetic normal fault (Fault 6). Similarly to the Curimã field, there are hydrocarbon accumulations in deep-water Ceará (Pecém discovery) and Potiguar Basins (Pitu discovery) that show combined plays, as presented by Maia de Almeida et al. (2020) and ANP (2017b). Aptian transitional reservoirs were trapped by a normal fault and an erosional unconformity. The Espoir and Baobab fields in Ivory Coast are also trapped by faulted blocks and the Albian unconformity (Kelly and Doust, 2016). These authors explained that reactivation of the inherited rift structures helped forming combined structural and stratigraphic traps.

The Jubilee Field in Ghana comprises a combination of structural and stratigraphic traps associated with the topography created by the transform tectonics during the opening of the Atlantic (Dailly et al., 2017). It is an Upper Cretaceous high-quality oil pay (Turonian in age) within a drift submarine fan sequence. In the Mundaú sub-basin, the combined plays occur in the Aptian transitional sequence. Nevertheless, the presence of more recent combined plays such as those at Jubilee cannot be ruled out in the Mundaú sub-basin as suggested by Maia de Almeida et al. (2020) and Leopoldino Oliveira et al. (2020), as well as in other basins of the

614 Equatorial Atlantic as exemplified by the Zaedyus field in French Guiana, considered an
615 analogous example of the African Jubilee field.
616
617 *5.2.2. Structural plays*
618 Well 4CES0128 was classified as a new discovery between the Curimã Fault and
619 Fault 8 (Table 1, Figs. 8a and 10). The Curimã Fault was capable of forming hanging-wall
620 blocks with broad anticline traps as the one reached by this well, i.e. a **structural play**. Close
621 to well 4CES0128, the Curimã Fault shows a relatively large offset, and Fig. 7a shows the
622 deposition of Uruburetama shales. This well proved that hanging-wall block and anticline traps
623 can be successful targets in the Mundaú sub-basin.
624 Jianping et al. (2010) presented different kinds of traps developed in different
625 strata controlled by different tectonic activities along the Côte d'Ivoire-Ghana transform
626 margin. They show that most are structural traps, such as fault-block and anticline traps. They
627 interpreted that anticline traps are related to the transform structures at the end of the St Paul
628 and Romanche Fracture Zones. The Espada field, crossed by well 4CES0143, comprises a
629 **stratigraphic play** composed of Upper Cretaceous turbiditic reservoirs occurring between
630 1,262 and 1,278 m (~1030 ms in the interpreted seismic volume). These reservoirs are located
631 close to Faults 1 and 2 (Figs. 8d and 10). These faults do not trap oil; instead, they are related
632 to the migration of oil into the Espada field. Such an interpretation takes into account that oil
633 accumulated in the Ubarana Formation was generated in the Paracuru Formation and used
634 faults as migration paths to turbidite sands in the Espada field (Costa et al., 1990). In addition,
635 well 4CES0128 also reached Upper Cretaceous pinched-out turbiditic sandstones forming a
636 stratigraphic trap (Fig. 8a and 10).
637 Recent and important discoveries have drawn the attention to these subtle traps
638 (Dolson et al., 2018; Ward et al., 2016; 2018). As an example, the Stabroek block in Guyana

639 includes several prosperous fields such as Liza, Payara, Liza deep, Snoek, Turbot, Pacora and
640 Mako fields. This block contains sediments of Amazonian origin, which were deposited by the
641 Guiana Current. There are multiple play types in this block, including Cretaceous and
642 amplitude-supported plays containing stratigraphic onlaps, turbidites and basin floor fans
643 (Offshore, 2020; Zhang et al., 2019). According to Zalán et al., (2019), the trapping mechanism
644 is invariably stratigraphic in nature, with lateral and updip pinch outs limiting the reservoirs
645 containing hydrocarbons. These authors are hopeful to replicate this success in the Foz do
646 Amazonas and Pará-Maranhão Basins.

647 In the BEM, Pelegrini and Severiano Ribeiro (2018) mapped turbiditic plays in
648 depositional pinch-outs (sandstones inside shales) in shallow and deep waters off Pará-
649 Maranhão. In deep-water Mundaú sub-basin, stratigraphic traps were created by depositional
650 pinch-outs and by volcanic bodies - turbiditic sandstones were interpreted as having reflectors
651 with high acoustic impedance contrasts, low frequency, lensoid geometry, and variable lateral
652 extension, ranging from 5 to 8 km (Leopoldino Oliveira et al., 2020).

653 Finally, the recent discoveries of the Pelican and Rossignol wells confirm that Upper
654 Cretaceous stratigraphic plays in the deep-water Tano Basin (Ghana) comprise prolific
655 reservoir intervals (Scarselli et al., 2018). Daily et al., (2013) also concluded about the
656 importance of stratigraphic plays in the Gulf of Guinea. Thus, the results presented here show
657 successful plays of Mundaú sub-basin that can be replicated in other parts of the Equatorial
658 South Atlantic, as well as in Equatorial Africa.

659

660 *5.3. Exploration Failures in the Mundaú sub-basin*

661

662 Unfortunately, some cases of exploration failures were recorded in the study area.
663 For example, wells 3CR0001 and 7CR0025 drilled strata between Faults 6 and 7 but failed to

664 find any hydrocarbons (Table 1 and Fig. 6). This means that a putative extension of the Curimã
665 field to the southeast cannot be confirmed due to the smaller thickness of Units 5 and 6 in this
666 region (Figs. 7a and 7b). The relatively minor thickness of Unit 5 can be related to widespread
667 erosion during the Aptian-Albian (Morais Neto et al., 2003; Condé et al., 2007; Brownfield
668 and Charpentier, 2006; Nemčok et al., 2016a), which removed part of this formation in the east
669 and southeast parts of the study area. In contrast, the observed thinning of Unit 6 can be
670 attributed to an erosional event of regional expression affecting Maastrichtian strata (Morais
671 Neto et al., 2003).

672 Well 1CES0115 was drilled between Faults 7 and 8, similarly to the successful well
673 4CES0128. However, due to the presence of a structural high in the east and southeast, Unit 5
674 was totally eroded close to well 1CES0115 (Figs. 5 and 7b). Although oil shows were found in
675 Unit 4, reservoir quality was poor. This well confirmed that basement faults controlled
676 deposition during the syn-rift and transitional stages, and that basinwide erosional events
677 contributed to the removal of prolific reservoir intervals in Unit 5.

678 Wells 3BRSA243 and 3CES0031A were drilled between Faults 5 and 6 with the
679 aim of verifying the southeast extension of the Curimã field. Yet, they were considered dry
680 (Table 1) and, based on the data in this work, we can infer that Fault 5 does not form a
681 competent seal. It is worth pointing out that transcurrent faults change their properties along
682 strike (Zalán, 1986). Well 3CES0031A was drilled in a region showing erosion of both Units
683 5 and 6 (Fig. 7), further decreasing its chance for success.

684 Well 1CES0030 was considered a wildcat; the aim was to test the footwall of the
685 Fault 5. Nevertheless, this well reached its fault zone, crossing Unit 5 on the hanging-wall
686 block and the Electric Mark 80 on the footwall (Fig. 8b). This well crossed clayey sandstones
687 of low permeability, with cataclasites in the fault zone reducing their grain size, porosity and
688 permeability. Clay minerals formed in the fault zone tend to compromise reservoir quality.

689 Furthermore, this well was drilled on the margin of a submarine channel incising Unit 6, the
690 main seal interval in the study area, a detail that may have led to the failure of well 1CES0030
691 as a wildcat.

692 This work correlated data with very different resolutions, e.g. seismic data (3D)
693 with a resolution of hundreds of meters and well data (1D) with a resolution of dozens of
694 centimeters. The different scales of seismic and well data do not permit a coherent assessment
695 of reservoir lateral continuity, considering that the main reservoir intervals in the Curimã and
696 Espada fields are thinner than 20 meters. Thus, one seismic reflection in the interpreted seismic
697 volume may represent several porous layers with reservoir potential. Accordingly, we can
698 suggest the future development of a 3D geological model of the area using sequence
699 stratigraphic concepts (e.g. Catuneanu, 2006; Martins-Neto and Catuneanu, 2010; Holz et al.,
700 2017). A 3D reservoir model using geostatistic numerical models should be used in a second
701 stage as a basis for simulation and fluid flow analysis (Consentino, 2001). These two
702 approaches will be crucial to plan the development of the oil fields referred to in this work.
703

704 **6 CONCLUSIONS**

705

706 Three-dimensional (3D) structural modelling integrating a seismic cube and well
707 data from the Mundaú sub-basin, including part of the Espada field and the entire Curimã field,
708 was developed in this research. This work introduced a variety of plays from an oil producing
709 region of the BEM expanding the possibility of future discoveries in this area, and also in the
710 Guyana-Suriname-French Guiana system and Equatorial Africa as a whole. The findings in
711 this research have focused on subtle stratigraphic traps. In addition, we also assess the
712 importance of structural and combined plays, challenging academia and industry to consider
713 these play types as crucial in Equatorial margins of the Central Atlantic; we emphasize here

714 that the historical distribution of the giant fields in all the world is 79% of structural plays
715 (Dolson et al., 2018). Main conclusions are as follows:
716
717 a) Extensional faults in the study area are planar at depth, seaward-dipping, and
718 revealing a NW-SE strike direction and a NE dip direction. They present an *en*
719 *echelon* geometry and are responsible for stepping and tilting of crustal blocks (half-
720 grabens) during the syn-rift phase. Furthermore, the faults were active until the
721 beginning of the drift phase. Some of them root into the basement while others reach
722 the top of Unit 1.
723
724 b) Seismic interpretation indicates transcurrent movement in the mapped faults,
725 recorded in the form of: abrupt change in seismic facies across faults; changes from
726 normal to reverse along their strike and with depth; changes in thickness and intensity
727 of seismic reflections across faults; and synclines and anticlines formed between
728 faults. Strike-slip tectonics reflects the nearby presence of transtensional fault
729 systems associated with oblique rifting of the Equatorial Atlantic.
730
731 c) In the study area are found important oil accumulations in combined, structural and
732 stratigraphic plays.
733 **Combined plays** are formed by Aptian reservoirs in block tilted by Faults
734 6 and 7, and the deposition of the transgressive shales of Unit 6 (Uruburetama Mb.)
735 above an erosional unconformity. It is worth stressing the importance of not completely
736 eroding the transitional Unit 5 (Paracuru Formation), which contains better reservoirs
737 in the study area, as well as the Uruburetama Member, sealing underlying reservoir
738 intervals. The basement structure controlled deposition during the syn-rift and

739 transitional stages. In addition, the structural high in the SE part of the area was largely
740 removed by an erosional event after the transitional phase, contributing to erosion of
741 the Unit 5 and, consequently, the failure of some exploratory wells. This type of play
742 is also found in the African conjugate margin represented by Espoir and Baobab fields
743 in Ivory Coast Basin.

744 **Structural plays** comprise anticlinal traps on the hanging-wall block tilted
745 by Fault 7 (Curimã Fault). The Côte D'Ivoire-Ghana transform margin presents this
746 type of play which is related to the transform structures at the end part of Fracture
747 Zones.

748 **Stratigraphic plays** consist of Upper Cretaceous turbidite sandstones
749 intercalated with shales. Here, faults are not important traps. However, they are
750 responsible for oil migration. Very important discoveries in Stabroek block in Guyana
751 and in Gulf of Guinea were assigned to this type of play.

752

753 d) In summary, the mapping of faults and traps in this work revealed the importance of
754 a multi-faceted structural component to the entrapment of hydrocarbons in the
755 Mundaú sub-basin. These results can assist further geological modelling in the BEM
756 and, consequently, reservoir simulations in order to plan the development of proven
757 and future oil fields. The structural model presented here is a starting point to further
758 exploration work in the remainder of the BEM and in the conjugate Equatorial Africa.

759

760 **Acknowledgements**

761 The authors are grateful to the Brazilian National Petroleum Agency for providing seismic and
762 well data, and to Schlumberger for their software licenses. The authors also thank Cardiff
763 University (3D Seismic Lab) and the Coordenação de Aperfeiçoamento de Pessoal de Nível

Superior (CAPES) for an exchange period of the first author in 2017, and the Federal University of Ceará (Laboratórios de Interpretação Sísmica e de Geologia Marinha e Aplicada) for their support to this study. This study was financed in part by CAPES, Brazil, Finance Code 001. The authors are grateful to the anonymous reviewers for their comments to earlier versions of this work.

7 REFERENCES

Alves, T.M., Cunha, T.A. 2018. A phase of transient subsidence, sediment bypass and deposition of regressive–transgressive cycles during the breakup of Iberia and Newfoundland. Earth and Planetary Science Letters, 484, 168-183.

Andrade, J.F.P., Gomes, M.P., Bezerra, F.R., Castro, D.L., Vital, H. 2018. Morphotectonic development of the Ceará Terrace: a marginal ridge on the western side of the Romanche Fracture Zone in the Brazilian Equatorial Margin. Geo-Marine Letters. Published on line: 12 July 2018. Doi:10.1007/s00367-018-0541-y.

ANP, 2013. Sumário Executivo do Campo de Espada. Contrato de Concessão n° 48000.003777/97-31. Plano de Desenvolvimento aprovado na Reunião de Diretoria n° 718 de 18/07/2013, Resolução de Diretoria n° 715/2013. 2 pp.

ANP, 2016. Sumário Executivo do Campo de Curimã. Plano de Desenvolvimento Aprovado. Reunião de Diretoria nº 812 de 07/08/2015, Resolução nº 584/2015. Agência Nacional do Petróleo, Gás Natural e Biocombustíveis (ANP). 3 pp.

ANP, 2017a. BACIA DO CEARÁ, Sumário Geológico e Setores em Oferta. Ildeson Prates Bastos. Superintendência de Definição de Blocos – SDB. Rodada 15. Brasil, Concessões de Petróleo e Gás. Agência Nacional do Petróleo, Gás Natural e Biocombustíveis (ANP). 17 pp.

ANP, 2017b. BACIA POTIGUAR, Sumário Geológico e Setores em Oferta. Carlos Mikael Arnemann Batista. Superintendência de Definição de Blocos – SDB. Rodada 15. Brasil, Concessões de Petróleo e Gás. Agência Nacional do Petróleo, Gás Natural e Biocombustíveis (ANP). 17 pp.

ANP, 2018. BACIA POTIGUAR. 15ª Rodada de Licitação da Agência Nacional do Petróleo, Gás Natural e Biocombustíveis. Superintendência de Definição de Blocos. Por Carlos Mikael Arnemann Batista.

ANP, 2020. Painel Dinâmico da Agência Nacional do Petróleo, Gás Natural e Biocombustíveis. http://www.anp.gov.br/exploracao-e-producao-de-oleo-e-gas/painel-dinamico-de-producao-de-petroleo-e-gas-natural.

Antobreh, A. A., Faleide, J. I., Tsikalas, F., and Planke, S.: Rift-shear architecture and tectonic development of the Ghana margin deduced from multichannel seismic reflection and potential field data, Mar. Petrol. Geol., 26, 345–368, doi:10.1016/j.marpetgeo.2008.04.005, 2009.

Antunes, A. F. 2004. Evolução tectono-estrutural do campo de Xaréu (Sub-bacia Mundaú, Bacia do Ceará – NE do Brasil): abordagem multiescala e pluriferramental. Tese de Doutorado, Programa de Pós-Graduação em Geodinâmica e Geofísica, Universidade Federal do Rio Grande do Norte, Natal. 376 p.

Antunes, A. F., Jardim de Sá, E.F., Araújo, R.G.S., Lima Neto, F.F. 2008. Caracterização tectonoestrutural do Campo de Xaréu (Sub-Bacia de Mundaú, Bacia do Ceará – NE do Brasil): abordagem multiescala e pluriferramental. Revista Brasileira de Geociências. 38(1 - suplemento): 88-105.

Attoh, K., Brown, L., Guo, J., Heanlein, J. 2004. Seismic stratigraphic record of transpression and uplift on the Romanche transform margin, offshore Ghana. Tectonophysics 378 (2004) 1 –16. doi:10.1016/j.tecto.2003.09.026

814 Azevedo, R.P. 1991. Tectonic evolution of Brazilian equatorial continental margin
815 basins. Imperial College London (University of London). Phd. Thesis. London, UK, 535 p.
816 Basile C., Mascle J., Guiraud R. 2005. Phanerozoic geological evolution of the
817 Equatorial Atlantic domain. Journal of African Earth Sciences, 43:275-282.
818 https://doi.org/10.1016/j.jafrearsci.2005.07.011
819 Beltrami, C. V., Alves, L. E. M., Feijó, F. J. 1994. Bacia do Ceará. In: Boletim de
820 Geociências da Petrobras, v.8, n.1, p. 117-125.
821 Brandes, C., Tanner, D.C. 2014. Fault-related folding: a review of kinematic
822 models and their application. Earth Sci. Rev. 138, 352–370.
823 Bridwell, R. J. 1975. Sinuosity of strike-slip fault traces. Geology, 3 (11): 630-632.
824 doi.org/10.1130/0091-7613(1975)3<630:SOSFT>2.0.CO;2.
825 Brooks, J., Glennie, K. W. 1987. Petroleum Geology of North West Europe,
826 Graham & Trotman, London.
827 Brownfield, M.E., Charpentier, R.R., 2006, Geology and total petroleum systems
828 of the Gulf of Guinea Province of west Africa: U.S Geological Survey Bulletin 2207-C, 32 p.
829 Castro, A. S. de. 1993. Arcabouço Estrutural e Evolucão Tectônica da Sub-Bacia
830 de Icaraí, Bacia do Ceará. Unpublished Master's thesis, Universidade Federal Ouro Preto,
831 Brazil.
832 Catuneanu, O. 2006. Principles of Sequence Stratigraphy. Elsevier, 375 pp.
833 Condé, V.C., Lana, C.C., Pessoa Neto, O.C., Roesner, E.H., Morais Neto, J.M.,
834 Dutra, D.C. 2007. Bacia do Ceará. In: Boletim de Geociências da Petrobras, Rio de Janeiro, v.
835 15, n.2, p. 347-355, maio/nov.
836 Consentino, L. 2001. Integrated Reservoir Studies. Institut Français du Pétrole
837 Publications. Editons Technip, Paris. 336 pp.

838 Corfield, S., Sharp, I. 2000, Structural style and stratigraphic architecture of fault
839 propagation folding in extensional settings: a seismic example from the Smørbukk area, Halten
840 Terrace, Mid-Norway: Basin Research, v. 12, no. 3-4, p. 329-341.
841 Costa, I.G., Beltrami, C.V., Alves, L.E.M. 1990. A evolução tectono-sedimentar e
842 o "habitat" do óleo na Bacia do Ceará. Boletim de Geociências da Petrobras, v.4, n.1, p. 65-74.
843 Dailly, P., Henderson, T., Hudgens, E., Kanschat, K., Lowry, P., 2013. Exploration
844 for cretaceous stratigraphic traps in the Gulf of Guinea, west Africa and the discovery of the
845 jubilee field: A play opening discovery in the Tano Basin, offshore Ghana. In: In: Mohriak,
846 W.U., Danforth, A., Post, P.J., Brown, D.E., Tari, G.C., Nemčok, M., Sinha, S.T. (Eds.),
847 Conjugate Divergent Margins, vol. 369. Geological Society, London, Special Publications, pp.
848 235–248. https://doi.org/10.1144/SP369.12.
849 Dailly, P., Henderson, T., Kanschat, K., Lowry, P., Sills, S. 2017. The Jubilee
850 Field, Ghana: Opening the Late Cretaceous Play in the West African Transform Margin.
851 Memoir 113: Giant Fields of the decade 2000-2010, 2017 (Chapter 14). AAPG Special
852 Volumes. Pages 257-272. DOI: 10.1306/13572010M1132997
853 Davison, I., Faull, T., Greenhalgh, J., Beirne, E.O., Steel, I., 2016. Transpressional
854 structures and hydrocarbon potential along the Romanche Fracture Zone: a review. In: In:
855 Nemčok, M., Rybar, S., Sinha, S.T., Hermeston, S.A., Ledvenyiova, L. (Eds.), Transform
856 Margins: Development, Controls and Petroleum Systems: London, vol. 431. Geological
857 Society, Special Publications, pp. 235–248.
858 Deng, Q., Wu, D., Zhang, P., Chen, S. 1986. Structure and deformational character
859 of strike-slip fault zones. Pure and applied geophysics. Volume 124, Issue 1–2, pp 203–223.
860 Dolson, J., He, Z., Horn, B.W. 2018. Advances and Perspectives on Stratigraphic
861 Trap Exploration-Making the Subtle Trap Obvious. Search and Discovery Article #60054

862 (2018). AAPG 2017 Middle East Region Geosciences Technology Workshop, Stratigraphic
863 Traps of the Middle East, Muscat, Oman, December 11-13, 2017. 67 pp.
864 Exxon Mobil. 2020. Guyana project overview. Article Feb. 5, 2020. Accessed on
865 May 09, 2020. https://corporate.exxonmobil.com/Locations/Guyana/Guyana-project-
866 overview#DiscoveriesintheStabroekBlock
867 Fossen, H. 2016. Structural Geology. Cambridge University Press, 2nd Edition,
868 ISBN: 978-1-107-05764-7. 452 pp.
869 Fossen, H., Teyssier, C., Whitney, D. L. 2013. Transtensional folding. Journal of
870 Structural Geology, v. 56, pp. 89-102.
871 Françolin, J.B.L., Szatmari, P. 1987. Mecanismo de rifteamento da porção oriental
872 da margem norte brasileira. Revista Brasileira de Geociências, 17:196-207.
873 Gorini, M. A., 1993, A margem equatorial brasileira: uma visão geotectônica:
874 Resumos expandidos do Congresso Internacional da Sociedade Brasileira de Geofísica 3:
875 Sociedade Brasileira de Geofísica, v. 2, p. 1355–1357.
876 Goss, S., D. Mosher, and G. D. Wach, 2008, Continental margin development of
877 the equatorial Atlantic gateway: Suriname, South America: Central Atlantic Conjugate
878 Margins Conference, Halifax, p. 282–291.
879 Hardman, R. F. P., Booth, J. E. 1991. The significance of normal faults in the
880 exploration and production of North Sea hydrocarbons. In: Roberts A. M., Yielding, G. &
881 Freeman, B. (eds), The Geometry of Normal Faults, Geological Society Special Publication
882 No 56, pp 1-13.
883 Heine, C., Brune, S. 2014. Oblique rifting of the Equatorial Atlantic: Why there is
884 no Saharan Atlantic Ocean. Geology (2014) 42 (3): 211–214. doi: 10.1130/G35082.1

885 Hempton, M. R., Neher, K. 1986. Experimental fracture, strain and subsidence
886 patterns over en échelon strike-slip faults: implications for the structural evolution of pull-
887 apart basins. Journal of Structural Geology. https://doi.org/10.1016/0191-8141(86)90066-0
888 Hoerlle, M. R., Gomes, C.J.S., Matos, R.M.D. 2007. O Graben de Apodi, região
889 sudoeste da bacia Potiguar, RN, uma interpretação com base em seções sísmicas e dados de
890 poços. R. Esc. Minas, Ouro Preto, 60(4): 593-602.
891 Holz, M. , Vilas-Boas, D.B., Troccoli, E.B., Santana, V.C., Vidigal-Souza, P.A.
892 2017. Conceptual Models for Sequence Stratigraphy of Continental Rift Successions.
893 Stratigraphy & Timescales. Vol. 2, Pages 119-186.
894 Howard, K.A., John, B.E., 1997. Fault-related folding during extension: plunging
895 basement-cored folds in the Basin and Range. Geology 25 (3), 223–226.
896 Huaicun, J. 2014. Progress and revelation of exploration of large oil and gas fields
897 around the globe. Sci. Technol. Rev., 32 (8) (2014), pp. 76-83
898 Illing, L. V., Hobson, G. C. 1981. Petroleum Geology of the Continental Shelf of
899 North-West Europe, institute of Petroleum, Heyden, London.
900 Jiang, H., Pang, X., Shi, H., Liu, L., Bai, J., Zou, S. 2015. Effects of fault activities
901 on hydrocarbon migration and accumulation in the Zhu I Depression, Pearl River Mouth Basin,
902 South China Sea. Australian Journal of Earth Sciences 62(6):775-788.
903 DOI10.1080/08120099.2015.1101400
904 Jianping, L., Xiaohua, P., Jun, M., Zuoji, T., Lunkun, W. 2010. Exploration targets
905 in the Côte d'Ivoire-Ghana transform margin in Equatorial West Africa. PETROL. EXPLOR.
906 DEVELOP., 2010, 37(1): 43–50.
907 Jin, G., Groshong, R. H. 2006. Trishear kinematic modeling of extensional fault
908 propagation folding: Journal of Structural Geology, v. 28, no. 1, p. 170-183.

Kelly, J., Doust, H. 2016. Exploration for Late Cretaceous turbidites in the Equatorial African and northeast South American margins. Netherlands Journal of Geosciences - Geologie en Mijnbouw, 95 – 4, 393–403. doi:10.1017/njg.2016.36

Khalil, S., McClay, K. 2002. Extensional fault-related folding, northwestern Red Sea, Egypt: Journal of Structural Geology, v. 24, no. 4, p. 743-762.

Knipe, R. J., Jones, G., Fisher, Q. J. 1998. Faulting, fault sealing and fluid flow in hydrocarbon reservoirs: an introduction. In: Jones, G., Fisher, Q. J., Knipe, R. J. (eds) Faulting, Fault Sealing and Fluid Flow in Hydrocarbon Reservoirs. Geological Society, London, Special Publications, 147, vii-xxi.

Lamarche, G., C. Basile, C., Mascle, J., Sage, F. 1997. The Côte d'Ivoire–Ghana transform margin: sedimentary and tectonic structure from multichannel seismic data. Geo-Marine Letters, 17: 62-69.

Leopoldino Oliveira, K.M., Bedle, H., Branco, R.M.G.C., de Souza, A.C.B., Nepomuceno Filho, F., Nomando, M.N., Maia de de Almeida, N., da Silva Barbosa, T.H., 2020. Seismic stratigraphic patterns and characterization of deepwater reservoirs of the Mundaú sub-basin, Brazilian Equatorial Margin. Mar. Pet. Geol. https://doi.org/10.1016/j.marpetgeo.2020.104310.

Lonsdale, P., 1989. Segmentation of the Pacific-Nazca spreading center, 1-DEGREESN-20-DEGREES-S. J. Geophy. Res.-solid Earth 94 (B9), 12197-12225. http://dx.doi.org/10.1029/JB094iB09p12197.

Macgregor, D.S., Robinson, J., Spear, G., 2003. Play fairways of the Gulf of Guinea transform margin. In: In: Arthur, T.J., Macgregor, D.S., Cameron, N.R. (Eds.), Petroleum Geology of Africa: New Themes and Developing Technologies, vol. 207. Geological Society, London, Special Publications, pp. 131–150. https://doi.org/10.1144/GSL.SP.2003.207.7.

Maia de Almeida N.M. , Alves, T.M., Nepomuceno Filho, F., Freire, G.S.S., Souza, A.C.B., Normando, M.N., Oliveira, K. M.L., Barbosa, T.H.S. 2020. Tectono-sedimentary evolution and petroleum systems of the Mundaú sub-basin: A new deep-water exploration frontier in equatorial Brazil. AAPG Bulletin, v. 104, no. 4 (April 2020), pp. 795–824. DOI:10.1306/07151917381

Martins-Neto, M.A., Catuneanu, O. 2010. Rift sequence stratigraphy. Marine and Petroleum Geology, 27(1):247-253.

Matos R.M.D., Waick R.N., Pimentel V.P.C. 1996. Bacia do Ceará (Mundaú): uma fase rifte convencional!? In: SBG/Núcleo Bahia-Sergipe, Congr. Bras. Geol., 39, Anais, 5:358-362.

Matos R.M.D. 2000. Tectonic evolution of the equatorial south Atlantic. In: Mohriak W., Talwani M. (Eds.). Atlantic rifts and continental margins, p. 331-354. Washington, D.C., American Geophysical Union.

Mcclay, K.R., Scott, A.D. Experimental models of hangingwall deformation in ramp-flat listric extensional fault systems. Tectonophysics, v.188, p. 85-96, 1991.

Medeiros, W.E. , Nascimento, A. F. , Antunes, A.F., Emanuel Ferraz Jardim de Sá, E.F.J., Lima Neto, F.F. 2007. Spatial pressure compartmentalization in faulted reservoirs as a consequence of fault connectivity: a fluid flow modelling perspective, Xaréu oil field, NE Brazil.

Milani E.J., Brandão J.A.S.L., Zalán P.V., Gamboa L.A.P. 2000. Petróleo na margem continental brasileira: geologia, exploração, resultados e perspectivas. Brazilian Journal of Geophysics, 18:352-396. http:// dx.doi.org/10.1590/S0102-261X2000000300012

Mitchum, R.M., Vail, P.R., Thompson, S. 1977. Seismic Stratigraphy and Global Changes of Sea Level, Part 2: The Depositional Sequence as a Basic Unit for Stratigraphic

958 Analysis. Seismic Stratigraphy Applied to Hydrocarbon Exploration. AAPG Memoir 26, 53-
959 62.

960 Mohriak W.U. 2003. Bacias sedimentares da margem continental brasileira. In:
961 Bizzi L.A., Schobbenhaus C., Vidotti R.M., Golçalves J.H. (Eds.). Geologia, tectônica e
962 recursos minerais do Brasil: textos, mapas & SIG, p. 87-165. Brasília, CPRM.

963 Morais Neto, J. M., Pessoa Neto, O. C., Lana. C. C., Zalán. P. V. 2003. Bacias
964 sedimentares brasileiras: Bacia do Ceará. Phoenix, Aracaju, v. 57, p. 1-6.

965 Moustafa, A. R., Abd-Allah, A. M. 1992. Transfer zones with en echelon faulting
966 at the northern end of the Suez Rift. Tectonics, AGU Journal. Volume 11, Issue 3, pages 499-
967 506. https://doi.org/10.1029/91TC03184

968 Nemčok M., Rybar, S., Odegard, M., Dickson, W., Pelech, O., Ledve´Nyiova, L.,
969 Matejova, M., Molc, M., Hermeston, S., Jones, D., Cuervo, E., Cheng, R., Forero, G. 2016a.
970 Development history of the southern terminus of the Central Atlantic: Guyana–Suriname case
971 study. From: Nemčok, M., Rybár, S., Sinha, S. T., Hermeston, S. A. & Ledvenyiova, L. (eds)
972 2016. Transform Margins: Development, Controls and Petroleum Systems. Geological
973 Society, London, Special Publications, 431, 145–178. First published online December 14,
974 2015, http://doi.org/10.1144/SP431.10

975 Nemčok, M., Rybár, S., Ekkertová, P., Kotulová, J., Hermeston, S. A., Jones, D.
976 2016b. Transform-margin model of hydrocarbon migration: the Guyana–Suriname case study.
977 From: Nemčok, M., Rybár, S., Sinha, S. T., Hermeston, S. A. & Ledvényiová, L. (eds) 2016.
978 Transform Margins: Development, Controls and Petroleum Systems. Geological Society,
979 London, Special Publications, 431, 199–217. First published online December 14, 2015,
980 http://doi.org/10.1144/SP431.6

981 Nemčok, M., Rybár, S., Sinha, S. T., Hermeston, S. A., Ledvényiova, L. 2016c.
982 Transform margins: development, controls and petroleum systems – an introduction. From:

983 Nemčok, M., Rybár, S., Sinha, S. T., Hermeston, S. A. & Ledvényiová, L. (eds) Transform
984 Margins: Development, Controls and Petroleum Systems. Geological Society, London, Special
985 Publications, 431, http://doi.org/10.1144/SP431.15
986 Nemčok, M. 2016d. Rifts and Passive Margins: Structural Architecture, Thermal
987 Regimes and Petroleum Systems. Cambridge University Press. 607 pp.
988 Offshore, 2020. https://www.offshore-technology.com/projects/liza-prospect-
989 development-stabroek-block/
990 OGJ, 2020. Oil and Gas Journal. ExxonMobil Confirms Oil Discovery in Second
991 Well Offshore Guyana, https://www.ogj.com/articles/2016/06/exxonmobil-confirms-oil-
992 discovery-in-second-well-offshore-guyana.html
993 Pellegrini, B.S., Severiano Ribeiro, H. J. P. 2018. Exploratory plays of Pará-
994 Maranhão and Barreirinhas basins in deep and ultra-deep waters, Brazilian Equatorial Margin.
995 Brazilian Journal of Geology, 48(3): 485-502. DOI: 10.1590/2317-4889201820180146
996 Pessoa Neto, O. C. 2004. Blocos basculados truncados por discordância angular:
997 lições aprendidas em trapeamento combinado de hidrocarbonetos, Bacia do Ceará, Nordeste
998 do Brasil. Boletim de Geociências Petrobras, Rio de Janeiro, v. 12, n. 1, p. 59-71.
999 Sauerbronn, J. L. B. 1996. Transição Crustal e Evolução Tectônica do Segmento
1000 Transformante da Margem Equatorial Brasileira, adjacente à Bacias de Barreirinhas e do Ceará.
1001 Master's thesis, Universidade Federal Ouro Preto, Brazil.
1002 Scarselli, N., Duval, G., Martin, J., Mcclay, K., Toothill, S. 2018. Insights into the
1003 Early Evolution of the Côte d'Ivoire Margin (West Africa). From: Mcclay, K. R. &
1004 Hammerstein, J. A. (eds) Passive Margins: Tectonics, Sedimentation and Magmatism.
1005 Geological Society, London, Special Publications, 476, https://doi.org/10.1144/SP476.8
1006 Sharp, I. R., Gawthorpe, R. L., Underhill, J. R., Gupta, S. 2000. Fault-propagation
1007 folding in extensional settings: Examples of structural style and synrift sedimentary response

1008 from the Suez rift, Sinai, Egypt: Geological Society of America Bulletin, v. 112, no. 12, p.
1009 1877-1899.
1010 Soares, D., Alves, T.M., Terrinha, P. 2012. The breakup sequence and associated
1011 lithospheric breakup surface: Their significance in the context of rifted continental margins
1012 (West Iberia and Newfoundland margins, North Atlantic). Earth and Planetary Science Letters,
1013 355-356, 311-326.
1014 Soares Júnior, A.V., Hasui, Y., Costa, J.B.S., Machado, F.B. 2011. Evolução do
1015 Rifteamento e Paleogeografia da Margem Atlântica Equatorial do Brasil: Triássico ao
1016 Holoceno. São Paulo, UNESP, Geociências, v. 30, n. 4, p. 669-692.
1017 Szatmari P., Françolin J.B., Zanotto O., Wolff S. 1987. Evolução tectônica da
1018 margem equatorial brasileira. Revista Brasileira de Geociências, 17:180-188.
1019 Tetteh, J. T. 2016. The Cretaceous Play of Tano Basin, Ghana. International
1020 Journal of Applied Science and Technology. Vol. 6, No. 1. February 2016. ISSN 2221-0997
1021 (Print), 2221-1004 (Online).
1022 Ward, N.I.P., Alves, T.M., Blenkinsop, T.G., 2016. Submarine sediment routing
1023 over a blocky mass-transport deposit in the Espírito Santo Basin, SE Brazil. Basin Research,
1024 30 (4): 816-834.
1025 Ward, N.I.P., Alves, T.M., Blenkinsop, T.G., 2018. Differential compaction over
1026 Late Miocene submarine channels in SE Brazil: Implications for trap formation. GSA Bulletin,
1027 130 (1-2), 208-221.
1028 Withjack, M. O., Olson, J., Peterson, E. 1990. Experimental models of extensional
1029 forced folds: AAPG Bulletin, v. 74, no. 7, p. 1038-1054.
1030 Watts, A. B., Rodger, M., Peirce, C., Greenroyd, C. J., Hobbs, R. W. 2009. Seismic
1031 structure, gravity anomalies, and flexure of the Amazon continental margin, NE Brazil.

JOURNAL OF GEOPHYSICAL RESEARCH, VOL. 114, B07103, doi:10.1029/2008JB006259

Yang, W. and Escalona, A. 2011. Tectonostratigraphic evolution of the Guyana Basin. AAPG Bulletin, v. 95, no. 8 (August 2011), pp. 1339–1368. DOI:10.1306/01031110106

Yielding, G. 1990. Footwall uplift associated with Late Jurassic normal faulting in the Northern North Sea, Journal of the Geological Society of London, 147, 219-222.

Zachariasen, J., Sieh, K. 1995. The transfer of slip between two en echelon strike-slip faults: A case study from the 1992 Landers earthquake, southern California. Journal Of Geophysical Research, Vol. 100, No. B8, Pages 15,281-15,301.

Zálan P. V., Warme, J. E. 1985. Tectonics and sedimentation of the Piauí-Camocim Sub-basins, Ceará Basin, Offshore Northeastern Brazil: Série Ciência-Técnica-Petróleo (17), Petrobras, Rio de Janeiro, 71 p.

Zalán, P. V. 1986. Identificação de falhas transcorrentes em seções sísmicas. Revista Brasileira de Geociências, 16 (3): 258-265.

Zalán P.V. 2004. Evolução fanerozóica das bacias sedimentares brasileiras. In: Mantesso-Neto V., Bartorelli A., Carneiro C.D.R., Brito Neves B.B.B. (Eds.). Geologia do continente sul-americano: evolução da obra de Fernando Flávio Marques de Almeida, p. 595-612. São Paulo, Editora Beca.

Zalán, P.V., 2015. Similarities and differences between magma-poor and volcanic passive margins – applications to the Brazilian marginal basins. In: Conference Paper - 14th International Congress of the Brazilian Geophysical Society held in Rio de Janeiro, Brazil, pp. 37–42. https://doi.org/10.1190/sbgf2015-007.

Zhang, G., Qu, H., Chen, G., Zhao, C., Zhang, F., Yang, H., Zhao, Z., Ma, M. 2019. Giant discoveries of oil and gas fields in global deepwaters in the past 40 years and the prospect

of exploration. Journal of Natural Gas Geoscience 4 (2019) 1-28. https://doi.org/10.1016/j.jnggs.2019.03.002